Micro-phytoplankton photosynthesis, primary production and potential export production in the Atlantic Ocean

Gavin H. Tilstone[1*], Priscila K. Lange[1,2,3†], Ankita Misra[4], Robert J. W. Brewin[1,5], Terry Cain[1].

[1]Plymouth Marine Laboratory, Prospect Place, West Hoe, Plymouth, PL1 3DH, UK.

[2]Federal University of Rio Grande, R. Sarmento Leite, 521, Porto Alegre - RS, 90050-170, Brazil.

[3]Department of Earth Sciences, University of Oxford, South Parks Road, Oxford, OX1 3AN, UK.

[4]CSIR - National Institute of Oceanography, Raj Bhavan Rd, Dona Paula, Goa, 403004, India.

[5] National Centre for Earth Observation, PML, Plymouth PL1 3DH, UK

*Corresponding author: ghti@pml.ac.uk

[†]Present address

Key Words : Micro-Phytoplankton, size-fractionated Primary Production, Atlantic Ocean, Export Production.

Abstract

Micro-phytoplankton is the >20μm component of the phytoplankton community and plays a major role in the global ocean carbon pump, through the sequestering of anthropogenic CO_2 and export of organic carbon to the deep ocean. To evaluate the global impact of the marine carbon cycle, quantification of micro-phytoplankton primary production is paramount. In this paper we use both *in situ* data and a satellite model to estimate the contribution of micro-phytoplankton to total primary production (PP) in the Atlantic Ocean. From 1995 to 2013, 940 measurements of primary production were made at 258 sites on 23 Atlantic Meridional Transect Cruises from the United Kingdom to the South African or Patagonian Shelf. Micro-phytoplankton primary production was highest in the South Subtropical Convergence (SSTC~409 ± 720 mg C m^{-2} d^{-1}), where it contributed between 38 % of the total PP, and was lowest in the North Atlantic Gyre province (NATL ~37 ± 27 mg C m^{-2} d^{-1}), where it represented 18 % of the total PP.

Size-fractionated photosynthesis-irradiance (*PE*) parameters measured on AMT22 and 23 showed that micro-phytoplankton had the highest maximum photosynthetic rate (P_m^B) (~5 mg C (mg Chl *a*)$^{-1}$ h^{-1}) followed by nano- (~4 mg C (mg Chl *a*)$^{-1}$ h^{-1}) and pico- (~2 mg C (mg Chl *a*)$^{-1}$ h^{-1}). The highest P_m^B was recorded in the NATL and lowest in the North Atlantic Drift Region (NADR) and South Atlantic Gyre (SATL). The *PE* parameters were used to parameterise a remote sensing model of size-fractionated PP, which explained 84% of the micro-phytoplankton *in situ* PP variability with a regression slope close to 1. The model was applied to the SeaWiFS time series from 1998 - 2010, which illustrated that micro-phytoplankton PP remained constant in the NADR, NATL, Canary Current Coastal upwelling (CNRY), Eastern Tropical Atlantic (ETRA), Western Tropical Atlantic (WTRA) and SATL, but showed a gradual increase in the Benguela Upwelling zone (BENG) and

South Subtropical Convergence (SSTC). The mean annual carbon fixation of micro-phytoplankton was highest in the CNRY (~140 g C m^{-2} yr^{-1}), and lowest in the SATL (27 g C m^{-2} yr^{-1}). A Thorium-234 based export production (ThExP) algorithm and applied it to estimates of total PP in each province. There was a strong coupling between micro-phytoplankton PP and ThExP in the NADR and SSTC where between 23 and 39 % of micro-phytoplankton PP contributed to ThExP. The lowest contribution by micro-phytoplankton to ThExP was in the ETRA and WTRA which were 15 and 21 % respectively. The results suggest that micro-phytoplankton PP in the SSTC is the most efficient export system and the ETRA is the least efficient in the Atlantic Ocean.

61 # 1. Introduction

62 Phytoplankton primary production (PP) is the principal engine of the biological pump that
63 determines the magnitude of CO_2 draw down from the atmosphere and export of fixed carbon
64 in the euphotic zone to the deep ocean. The efficiency of the biological pump and the fate of
65 fixed CO_2 remaining in or sedimenting out of the euphotic zone, depends on the physico-
66 chemical properties of the epipelagic system and its modification by the dominant trophic
67 food web in the ecosystem (Jochem & Zeitzschel, 1993). The size structure and taxonomic
68 composition of the phytoplankton community in the open ocean are important factors in
69 regulating sedimentation of algal cells and carbon export (Bienfang, 1981).

70 The smallest phytoplankton, known as the pico-phytoplankton (0.2 - 2 μm in size) are
71 a major component of the phytoplankton community and present in all oceanic systems,
72 dominating the low Chlorophyll-*a* (Chl *a*) biomass areas of sub-tropical and tropical regions
73 (Veldhuis, Timmermans, Croot & van der Wagt, 2005), both in terms of phytoplankton
74 biomass (Partensky, Hess & Vaulot, 1999) and PP (Bell & Kalff, 2001). Pico-phytoplankton
75 is efficient at fixing carbon, but this becomes limited by the availability of dissolved organic
76 nutrients in oligotrophic regions (Biller, Berube, Lindell & Chisholm, 2015; Grob, Jardillier,
77 Hartmann, Ostrowski, Zubkov et al., 2015). The trophic pathway of pico-phytoplankton, is
78 through an efficient microbial loop which recycles organic carbon within lower trophic
79 groups (heterotrophic bacteria, nano-flagellates, ciliates, heterotrophic dinoflagellates) so that
80 little is available for export (Azam, 1998; Kiorboe, 1993). By contrast, the micro-
81 phytoplankton which inhabit nutrient replete waters can act as ballast for transporting
82 atmospheric CO_2 to the deep ocean (Cho & Azam, 1988; Eppley & Peterson, 1979;
83 Falkowski, Barber & Smetacek, 1998). According to Stoke's Law, the micro-phytoplankton,
84 (>20μm) are expected to sink fast and represent a major vertical flux of carbon in epipelagic
85 systems to the deep ocean (Cushing, 1989; Dugdale & Goering, 1967; Legendre & Lefevre,

1989). This can occur as spectacular episodic, seasonal events in aggregates or flocs such as marine snow. Sedimentation rates of pico-phytoplankton and to a lesser extent the nano-phytoplankton (2-20 μm in size), except coccolithophorids, are considered to be negligible (Sarthou, Timmermans, Blain & Treguer, 2005) since much of this biomass is recycled in the photic zone (Chisholm, 1992; Kiorboe, 1993; Raven, 1998). Micro-phytoplankton is comprised of diatoms, dinoflagellates and colony forming cyanobacteria such as *Trichodesmium* spp.. Diatoms are one of the predominant contributors to global carbon fixation and export, accounting for 40% of the total PP in the Global Ocean (Mann, 1999; Smetacek, 1999; Treguer & Pondaven, 2000), and make a significant contribution to the biogeochemical cycling of nitrogen, phosphorus, and silicon (Nelson, Treguer, Brzezinski, Leynaert & Queguiner, 1995; Treguer, Nelson, Vanbennekom, Demaster, Leynaert et al., 1995). Within the micro-phytoplankton, the diatoms are believed to make the largest contribution to export production (ExP), potentially acting as a vector for POC export due to their ballasted armoury and palatability to higher trophic levels (Treguer & Pondaven, 2000).

Dinoflagellates are ubiquitous in the global ocean (Beardall & Raven, 2004), as either autotrophic life forms, that contribute directly to the biological carbon pump, or as heterotrophs that graze other phytoplankton. Species such as *Ceratium* spp. has a comprehensive biogeographic distribution from the warmest waters of the tropics to the coldest waters of the Polar Regions (Dodge & Marshall, 1994). Blooms of *Ceratium* spp. form a major component of both the total biomass and PP (Dodge & Marshall, 1994) and have expanded northwards in the Atlantic Ocean as a result of global warming (Hays, Richardson & Robinson, 2005). Some dinoflagellates enhance the degradation of faecal pellets in the euphotic zone, thus reducing the potential for ExP (Svensen, Morata & Reigstad, 2014).

The colonial marine cyanobacterium *Trichodesmium* spp. is found throughout the subtropical and tropical gyres of the Atlantic Ocean (Capone, Burns, Montoya, Subramaniam, Mahaffey et al., 2005) and has the ability to fix nitrogen from the atmosphere having a major impact on nitrogen cycling in the ocean (Grosskopf, Mohr, Baustian, Schunck, Gill et al., 2012; Olson, McGillicuddy, Flierl, Davis, Dyhrman et al., 2015).

In the Atlantic Ocean, the highest phytoplankton biomass and productivity occurs in the upwelling zones of the CNRY and BENG when micro-phytoplankton dominate the phytoplankton community under nutrient replete conditions. Rates of carbon fixation are reported to be between 500 and 6000 mg C m^{-2} d^{-1} (Tilstone, Smyth, Poulton & Hutson, 2009). Micro-phytoplankton and nano-phytoplankton dominate the NADR during bloom conditions when PP is reported to be between 500-800 mg C m^{-2} d^{-1}. Outside of these events, the pico-phytoplankton account for 78-90% of chlorophyll and 83-98% of primary production, when *Synechococcus* spp. dominate the community (Jochem & Zeitzschel, 1993).

Similarly in the NATL, pico-phytoplankton make the highest contribution to Chl *a* and PP (Maranon, Holligan, Varela, Mourino & Bale, 2000; Zubkov, Sleigh & Burkill, 2000), though a significant proportion of the total PP is attributed to nano- and micro-phytoplankton (Maranon, Holligan, Barciela, Gonzalez, Mourino et al., 2001; Maranon et al., 2000), which is determined by changes in nutrient supply to the euphotic zone (Maranon, Behrenfeld, Gonzalez, Mourino & Zubkov, 2003).

In the equatorial provinces of the Western and Eastern Tropical Atlantic (ETRA & WTRA), elevated phytoplankton biomass and primary productivity can occur as persistent year round phenomena (Perez, Fernandez, Maranon, Serret & Garcia-Soto, 2005a; Perez, Fernandez, Maranon, Serret, Varela et al., 2005b) due to the presence of Equatorial upwelling. The phytoplankton community is still dominated by pico-phytoplankton (Perez et al., 2005b; Zubkov, Sleigh, Tarran, Burkill & Leakey, 1998), but nano-phytoplankton

(Tarran, Heywood & Zubkov, 2006), diatoms and dinoflagellates increase in abundance at the peak of upwelling (Barlow, Aiken, Holligan, Cummings, Maritorena et al., 2002; Barlow, Aiken, Moore, Holligan & Lavender, 2004; Gibb, Barlow, Cummings, Rees, Trees et al., 2000).

Since micro-phytoplankton potentially contribute most to export production, quantifying its contribution to total PP is fundamental to improving our understanding of the carbon cycle and the biological pump. In this paper we address the following questions: What is the magnitude of micro-phytoplankton PP in open ocean provinces of the Atlantic Ocean? What is the contribution of micro-phytoplankton PP to total PP? How does the rate of micro-phytoplankton photosynthesis compare with that of nano- and pico-phytoplankton? Can accurate satellite models of micro-phytoplankton PP be developed for the Atlantic Ocean and if so, have there been recent changes in micro-phytoplankton PP? What is the contribution of micro-phytoplankton PP to export production?

2. Methods

2.1. Study area and sampling

From 1995 to 2013, 940 size-fractionated P_z measurements using simulated *in situ* incubations (SIS) were made at 258 stations on 10 Atlantic Meridional Transect Cruises (Fig. 1A, B, Table 1). In addition, size fractionated photosynthesis-irradiance (PE) curves were made at 62 stations at two depths in the water column (surface and DCM) on AMT22 in 2012 and AMT23 in 2013 (Fig. 1C). Of the 21 cruises listed in Table 1, we grouped them into two sets, based on the seasons in which the North and South Atlantic Gyres were sampled. The first group is comprised of cruises in boreal spring (Fig. 1A) and the second group consisted of cruises in boreal autumn (Fig. 1B).

158 A SeaBird SBE19+ CTD was deployed at each station to initially assess the vertical
159 structure of temperature, salinity, density, fluorescence and PAR and to collect the samples
160 for the P_z and PE curve measurements. For SIS P_z, seawater samples were collected in 10 L
161 black out carboys from light depths based on the PAR profiles. Depths for the PE curves
162 were determined from fluorescence profiles. Under conditions of vertical heterogeneity in the
163 fluorescence data, additional samples were taken at depths delineating strong changes in the
164 vertical profile. Mixed layer depth (MLD) was calculated as the depth at which the difference
165 with the surface density was greater than 0.125 kg m^{-3} (Levitus 1982). The mean sections of
166 temperature, salinity, Chl *a* fluorescence and primary production were calculated from
167 weight-averaged spatial interpolation of observations and plotted using the software Ocean
168 Data View (Fig. 2, 3).

169

170 *2.2. Size fractionated Chlorophyll-a.*

171 During AMT22 and 23, 200–300 mL samples were sequentially filtered through 10, 2 and 0.2
172 µm polycarbonate filters. After filtration, pigments were extracted in 90% acetone at -20 ºC
173 for 24 h after which the Chl *a* concentration was determined on a Trilogy Turner Design
174 Fluorometer using the method of Welschmeyer (1994). For each cruise, the fluorometer was
175 pre-calibrated and post-calibrated with a pure Chl *a* standard. The total Chl *a* concentration
176 was calculated as the sum of the three size fractions.

177

178 *2.3. Size fractionated phytoplankton photosynthesis and primary production*

179 For simulated *in situ* primary production on cruises AMT1-23, water samples were taken
180 from pre-dawn (03:15-05:15 GMT) deployments of SeaBird CTD rosette sampler on a
181 stainless steel frame with 21 x 10L and 3 x 20L niskin bottles. Samples were taken from 6-8

depths in the euphotic zone following the methods described in Tilstone et al. (2009). The samples were transferred from Niskin bottles to black carboys to prevent shock to the photosynthetic lamellae of the phytoplankton cells. Water from each sample was sub sampled into three 75 ml clear polycarbonate bottles and three black polycarbonate bottles. All bottles were pre cleaned following JGOFS protocols (IOC, 1994), to reduce trace metal contamination. Each sample was inoculated with between 185 and 555 kBq (5 - 15 µCi) $NaH^{14}CO_3$ according to the biomass of phytoplankton. The polycarbonate bottles were transferred to an on deck (*simulated in situ*) incubation system using neutral density and blue filters to simulate subsurface irradiance over depth to 97%, 55%, 33%, 20%, 14%, 7%, 3%, 1% or 0.1% of the surface value and incubated from local dawn to dusk (10 – 16 h). On AMT 1-11 bottles were incubated for 6h and carbon fixation over this period was scaled to daily PAR to calculate PP (Tilstone et al., 2009). The incubators were maintained at surface temperature by pumping sea water from a depth of ~7 m through the upper light level incubators (97, 55, 33, 14, & 7 %) and from a chiller maintained at ±1°C of *in situ* temperature for the lower light level incubators (3, 1 & 0.1%). For AMT 2-6 and 18-23, to terminate the incubations, suspended material were filtered sequentially through 0.2, 2 and 10 or 20 µm polycarbonate filters to measure the pico-, nano- and micro-phytoplankton production, respectively (for further details see Table 1). The filters were exposed to concentrated HCl fumes for 8-12 h immersed in scintillation cocktail and ^{14}C disintegration time per minute (DPM) was measured on board using a Perkin Elmer, Tricarb 2900 liquid scintillation counter and the external standard and the channel ratio methods were applied to correct for quenching.

On AMT22 and 23, photosynthesis-irradiance (*PE*) curves were measured at 62 stations at the surface and DCM, using linear photosynthetrons following the methods given in Tilstone, Figueiras, Lorenzo and Arbones (2003), with either 35 or 50 W tungsten halogen

or 9 W LED lamps depending on the ambient PAR at depth. For each depth, 16 aliquots of 70 mL were inoculated with 185 to555 kBq (5-15 μCi) of ^{14}C-labelled bicarbonate. Samples were maintained at *in situ* temperature during the 1.5 h incubations and were then sequentially filtered through 0.2, 2 and 10 μm polycarbonate filters. The filters were then exposed to 37% fuming hydrochloric acid and DPM was measured on board using the Tricarb 2900 Perkin Elmer scintillation counter as above. Natural ^{12}C carbon fixation within each sample was calculated following Tilstone et al. (2003). The spectral irradiance $Eq(\lambda)$ of the tungsten halogen and LED lamps were measured using a SATLANTIC HyperSAS radiometer (Model No. SATHSE0258) and the photosynthetic available radiation (E_{PAR}) at each bottle position in the photosynthetron were measured. Raw values of the initial slope of the photosynthesis-irradiance curve (α^B) are biased due to the emission spectrum of the light source. This bias was corrected by multiplying each α^B value by a weighting factor, computed as the ratio of the mean absorption spectrum of a particular size class to the weighted (by the emission spectrum of the light source) absorption spectrum of the same size class of phytoplankton. Further details of this correction are given in Brewin et al. (this issue). The spectral light saturated chlorophyll-specific rate of photosynthesis for each size class (P_m^B), and α^B, the light saturation parameter (E_k) and the rate of photoinhibition (β) were then estimated by fitting the normalised size-fractionated data to the model of Platt, Gallegos and Harrison (1980) as long as the $r^2 \geq 0.9$.

2.4. Satellite models of micro-phytoplankton primary production and export production.

Total water column integrated PP was computed using the wavelength resolving model (WRM) of Morel (1991) implemented following Smyth, Tilstone and Groom (2005) for the SeaWiFS time series. The WRM was chosen as it is known to be accurate for the Atlantic

231 Ocean (Campbell, Antoine, Armstrong, Arrigo, Balch et al., 2002; Carr, Friedrichs, Schmeltz,
232 Aita, Antoine et al., 2006; Friedrichs, Carr, Barber, Scardi, Antoine et al., 2009; Saba,
233 Friedrichs, Carr, Antoine, Armstrong et al., 2010; Tilstone et al., 2009). The % of size-
234 fractionated pico-, nano- and micro-phytoplankton PP were calculated from the model
235 described in Brewin et al. (this issue). This is an available light PP model and similar to that
236 of Platt et al. (1980). It computes the carbon fixation of pico- (<2μm), nano- (2-10μm) and
237 micro-phytoplankton (>10μm) cells. The model estimates the vertical Chl *a* profile as a
238 function of the surface concentration derived from satellite data, following methods modified
239 from Platt and Sathyendranath (1988) and (Uitz, Claustre, Morel & Hooker, 2006) re-
240 parameterised to AMT pigment profiles, then partitions Chl *a* into the three size classes using
241 the model of Brewin, Sathyendranath, Tilstone, Lange and Platt (2014). The model estimates
242 the euphotic depth following the approach of Morel et al., (2007), which modulates vertical
243 changes in the diffuse attenuation coefficient using the Chl *a* profile. For estimation of size
244 fractionated PP, the method of Uitz et al. (2008) was re-tuned using size-fractionated
245 photosynthesis-irradiance experiments on AMT 22 and 23, P_m^B and α^B measured for a flat
246 incident spectral light field are modelled separately for each size class. These parameters are
247 used to compute PP at each depth, at hourly intervals over the day length, for each size class.
248 These values are summed and integrated to give daily PP. A thorough sensitivity and error
249 propagation analysis on the model was conducted using Monte Carlo techniques to assess the
250 impact of uncertainty in the model input (e.g. Chl *a*, irradiance) and model parameters (e.g.
251 P_m^B, α^B) on the resulting computed PP. For further details of the model and uncertainty
252 analysis are given in Brewin et al. (this issue). Together with estimates of the light field,
253 derived from satellite estimates of photosynthetically available radiation (PAR) and the
254 diffuse attenuation of PAR, % PP for each size class were computed for each month from
255 1998 to 2010 using the SeaWiFS data. The PP of each size fraction was calculated from the

total PP using the WRM as a function of the % PP for each size class, which were integrated over the water column to 0.1% euphotic depth which was derived from K_{PAR} calculated as a function of Chl *a* .

We also used the algorithm of Henson, Sanders, Madsen, Morris, Le Moigne et al. (2011) to estimate ExP in each Atlantic province. This algorithm is derived from a comprehensive database of thorium-234 (^{234}Th) based particulate organic carbon (POC) export measurements (ThExP) and sea surface temperature (SST) whereby the ^{234}Th export ratio (*ThE*-ratio) = 0.23 * $\exp^{(-0.08*SST)}$. We applied the *ThE*-ratio to monthly estimates of total PP from the WRM to calculate daily, mean monthly and annual rates of ExP, which we compared with micro-phytoplankton PP.

3. Results

3.1. Hydrographic conditions

Mean sections of temperature, salinity and fluorescence for cruises in boreal spring and boreal autumn are given in Figure 2. In the Northern portion of the sections during boreal spring, colder (~16 °C) and less saline (36 psu) water (Fig. 2A, B) characterised the North Atlantic Drift (NADR) province (Fig. 1D), when the phytoplankton biomass reached >0.6 mg m^{-3} Chl *a* (Fig. 2C). During boreal autumn, the surface water temperature was higher (Fig. 2D) and the phytoplankton biomass was lower (Fig. 2F). At the southernmost extent of the NADR during boreal spring, a subtropical front marked the boundary between NADR and NATL province, where in the top 100 m of the water column the salinity increased to 37 psu, temperature increased to ~17 °C, and surface Chl *a* decreased to <0.5 mg m^{-3}. In boreal autumn, the temperature change from the NADR to the NATL was 18 – 20 °C. Further south in the WTRA the temperature rose to 28 °C, salinity increased to >37 psu when sub-surface

Chl *a* was <0.5 mg m^{-3} during boreal spring, and decreased to 35 psu when sub-surface Chl *a* was >1.0 mg m^{-3} during boreal autumn. In the southern hemisphere during boreal spring, an increase in sea surface temperature to >25 °C and an increase in salinity to 37 psu demarked the SATL province, where surface Chl *a* reached the lowest concentrations along the entire transect. During boreal autumn, temperatures in the SATL were lower, the salinity was similar and Chl *a* was higher. South of 35 °S, the temperature decreased to 16 °C and the salinity was <36 psu, and there was a concomitant increase in Chl *a* to >1.0 mg m^{-3}, characterizing the SSTC province. During boreal autumn, both the temperature (15 °C) and salinity (35.5 psu) were lower and Chl *a* was higher (>1.0 mg m^{-3}).

3.2. Simulated in situ size-fractionated primary production

Of the 21 AMT cruises used in this study, only 10 cruises measured micro-phytoplankton PP. On AMT 2-6 this was done using 20 µm filters, whereas on cruises AMT 18-23 used 10 µm filters (Table 1). During both boreal spring and autumn, depth specific-primary production (P_z) was highest in the surface waters of the NADR, WTRA and SSTC and lowest in the NATL and SATL (Fig. 3A, D). P_z was generally higher during boreal spring compared to autumn, especially in the NATL due to the closer proximity to the Mauritanian Upwelling of the CNRY on AMT 1-11 (Fig. 1A). The % contribution of micro-phytoplankton P_z to total P_z (Fig. 3B, E) was highest at the extreme ends of the transect, especially in boreal spring at ~100 m due to the influence of water column mixing and possibly the sedimentation of large aggregates. In the top 50 m, % micro-phytoplankton *Pz* reached ~30% in the NADR and NATL, but decreased to 15-30% in the WTRA and SATL. Below 50 m, the distribution of % micro-phytoplankton *Pz* was patchy with higher values at 100 m in the WTRA and at the boundary between the SATL and SSTC (Fig. 3B, E). The % contribution of pico-

304 phytoplankton P_z to total P_z was generally greater over the entire transect during both boreal
305 and autumn, and especially in the DCM during boreal autumn where % pico- phytoplankton
306 P_z was >60% (Fig. 3C, F).

307 Integrated *in situ* water column primary production (PP) from AMT1-11 and AMT18-23
308 for each size fraction and as a mean and mean % of the total, are given in Table 2. The actual
309 data for each size class and as a % of the total from AMT18-23 are given in Figure 4. Micro-
310 phytoplankton PP was highest in the SSTC (409 ± 720 mgC m^{-2} d^{-1}), where it contributed
311 38% of the total PP and was lowest in the NATL (37 ± 27 mgC m^{-2} d^{-1}) where it represented
312 18 % of the total PP (Table 2). Similarly, the highest pico-phytoplankton PP was in the SSTC
313 (mean ~309 ± 185 mgC m^{-2} d^{-1}) and WTRA (mean ~212 ± 115 mg C m^{-2} d^{-1}), which
314 contributed 28 and 60 % to the total PP and the lowest was in the SATL (Table 2). The
315 highest micro-phytoplankton PP were measured on AMT 18 in 2008 and AMT23 in 2013 at
316 the boundaries between the WTRA & NATL and SATL & SSTC. By comparison, pico-
317 phytoplankton PP was highest during AMT22 in 2012. Nano-phytoplankton PP was similar
318 throughout all cruises and on average represented 32% of the total PP in the Atlantic Ocean
319 (Table 2, Figure 4).

320

321 *3.3. Size-fractionated photosynthesis-irradiance parameters*

322 The variability in P_m^B, α^B and E_k during AMT22 and 23 for micro-, nano- and pico-
323 phytoplankton in surface waters and at the DCM are given in Figures 5, 6 and Table 3. In all
324 provinces and in both surface waters and the DCM, pico-phytoplankton had the highest Chl *a*
325 concentrations with ~0.1 mg m^{-3} at surface and ~0.25 mg m^{-3} at the DCM and micro-
326 phytoplankton had the lowest Chl *a* with ~0.02 mg m^{-3} at the surface and ~0.03 mg m^{-3} at the
327 DCM (Table 3). Micro-phytoplankton P_m^B was generally higher at the surface than in the

328 DCM in the NATL, SATL and SSTC (mean ~5.8 mg C (mg Chl-*a*)$^{-1}$ h^{-1}) and was similar
329 between the surface and DCM in the NADR and WTRA (NADR mean ~2.82; WTRA mean
330 ~5.4 mg C (mg Chl-*a*)$^{-1}$ h^{-1}; Fig. 5A, D, 6A, D, Table 3), probably as a result of more vertical
331 mixing in these provinces and the proximity of the DCM to the surface (Fig. 2). There was
332 considerable variability in P_m^B between cruises (Fig. 5, 6). In surface waters, micro-
333 phytoplankton had the highest P_m^B in the NATL during AMT22, followed by the WTRA and
334 SATL during AMT23 (Fig. 5A, D, Table 3). Additionally, when comparing size fractions,
335 micro-phytoplankton P_m^B > nano- P_m^B > pico- P_m^B, except in the WTRA where nano-
336 phytoplankton had the highest P_m^B (Table 3), especially during AMT23 (Fig. 5D). In the
337 DCM of the NATL and WTRA, micro-phytoplankton had the highest P_m^B, during both
338 AMT22 and 23 (Fig. 6A, D), and micro-phytoplankton P_m^B > nano- P_m^B > pico- P_m^B. In the
339 NADR, SATL and SSTC, however, nano-phyoplankton P_m^B > micro- P_m^B > pico- P_m^B,
340 especially on AMT23 (Fig. 6D). Pico-phytoplankton consistently had the lowest P_m^B at both
341 surface and the DCM, and in surface waters highest values were measured in the WTRA and
342 in the DCM in the SSTC.

343 Micro-phytoplankton α^B was similar between surface and DCM, highest in the WTRA
344 and lowest in the SSTC (Fig. 5B, E, 6B, E, Table 3). Only in surface waters of the WTRA
345 was micro-phytoplankton α^B > nano- α^B > pico- α^B, whereas in the other provinces (except
346 the NATL), pico- α^B > micro- α^B > nano- α^B. In the DCM, in all provinces except the NATL,
347 micro-phytoplankton had the highest α^B, reflecting the low light acclimation at depth. By
348 contrast, in the NATL nano-phytoplankton had the highest α^B.

349 The trend in P_m^B reflected E_k, such that micro-phytoplankton had the highest values at
350 both the surface and the DCM, with micro- E_k > nano- E_k > pico- E_k in the NADR & NATL
351 (Fig. 5C, F, 6C, F Table 3), indicating the adaptation of the larger size class to a higher light
352 environment in these provinces. By contrast, in the SATL, SSTC, and DCM of the WTRA,

353 nano- E_k > micro- E_k > pico- E_k, whereas in the surface waters of the WTRA nano- E_k > pico-
354 E_k > micro- E_k.

355

356 *3.4. Satellite estimates of micro-phytoplankton primary production.*

357 In Figure 8, we plot daily *in situ* and satellite estimates of micro-phytoplankton PP using
358 SeaWIFS data for cruises AMT18 – 23 (see Brewin et al. this issue for details on match-up
359 procedure). From AMT18 in 2008 to AMT23 in 2013 there were 26 satellite match-ups and
360 over all cruises there was a good agreement with *in situ* micro-PP in $1og_{10}$-space with 85% of
361 the variability explained, a slope close of ~0.69 and a low bias (-0.1) and centre-pattern root
362 mean square (0.3). The relative percentage difference (RPD) between *in situ* and satellite
363 estimates of micro-PP was 37 %. There were two match-up points in the SSTC on AMT 22
364 however, which exhibited large differences compared to *in situ* micro-phytoplankton PP
365 values (Fig. 7D). These data points were at the boundary of the SSTC and SATL, which are
366 very heterogeneous between low to high productive waters, so the difference in measurement
367 resolution (point value for in situ versus 4km x 4km pixel for satellite) may explain the
368 differences observed. If these points were removed, 90% of the variability explained, the
369 slope is closer to 1 (~0.78), root mean square is lower (0.28) and the RPD was reduced to 14
370 %, however nearly all of the remaining matchups were in a low PP range.

371 After applying this model to the SeaWiFS time series, we then extracted mean monthly
372 total and micro-phytoplankton PP in each province (Fig. 8). The seasonal oscillation between
373 maximum values in spring and minimum values in winter is well defined for both total and
374 micro-phytoplankton PP, especially in the temperate provinces of the NADR and SSTC (Fig.
375 8A, H). In the NADR, NATL, CNRY, ETRA, WTRA and SATL micro-PP remained
376 constant over the decadal time series (Fig. 8E, F). In the BENG and SSTC, there was a
377 significant increase in micro-PP from 1998 to 2010 (Fig. 8G, H; BENG, $F_{1,151} = 25.08$, $P <$

0.0001; SSTC, $F_{1,151}$ = 41.62, P < 0.0001). The cumulative values reflected the anomalies, with little change from 1998 to 2010 in the NADR, NATL, CNRY, ETRA, WTRA and SATL, except for a large decrease in micro-PP (increase in the NADR) during 2000 (Fig. 9). Similarly in the BENG and SSTC there was a progressive increase in the cumulative sum of micro-PP from 2001 to 2011 (Fig. 9G, H).

3.5. Satellite estimates of export production.

The algorithm of Henson et al. (2011) was applied to satellite estimates of total PP to estimate the average ThExP, which was 13 g C m^{-2} y^{-1} in the NADR and 16 g C m^{-2} y^{-1} and in the SSTC. In the NATL, SATL and WTRA the average annual ThExP was similar at 5, 4 and 5 g C m^{-2} y^{-1}, respectively and in the ETRA this increased to 8 g C m^{-2} y^{-1}. The largest mean annual ThExP is in the CNRY and BENG, which were 21 and 17 g C m^{-2} y^{-1}.

Comparing ThExP in each Atlantic province with the estimates of micro-phytoplankton PP, we found that in the NADR and SSTC ThExP is 23 and 39 % of micro-phytoplankton PP (Fig. 10A, D). By contrast, in the NATL and SATL the average annual ThExP is 14 and 15 % of the micro-phytoplankton PP, respectively (Fig. 10B). Similarly in the WTRA the average annual ThExP is 10 % of micro-phytoplankton PP, and in the ETRA it is 11 % (Fig. 10C). The ThExP of the CNRY and BENG, represent 15 and 21 % of micro-phytoplankton PP, respectively (Fig. 10A, D). We found that ThExP in the NATL and SATL was relatively constant (Fig. 11B, F), the NADR exhibited a decline until 2005, after which there as increase in ThExP (Fig. 11A) and the BENG and SSTC were constant until 2007 after which time ThExP increased to 2009 and decreased again in 2010 (Fig. 11G, H). The ETRA and WTRA displayed cyclical oscillations at 3-4 y scales between increases and decreases in ThExP (Fig. 11D, E). In the NATL, CNRY, ETRA and WTRA, there was un-

coupling between ThExP and micro-phytoplankton PP in 2000 which was repeated in the CNRY, ETRA and WTRA in 2009 (Fig. 11B, C, D, E).

4. Discussion

4.1. Variability in micro-phytoplankton primary production.

Pico-phytoplankton dominate the biomass and primary productivity in sub-tropical and tropical oligotrophic regions of the Atlantic Ocean (Maranon et al., 2000; Zubkov et al., 2000; Zubkov et al., 1998), however a significant proportion of this productivity is attributed to both the nano- and micro-phytoplankton (Maranon et al., 2001; Poulton, Holligan, Hickman, Kim, Adey et al., 2006). Spatial and temporal changes in nutrient and light availability, turbulence and predation affect the composition of the phytoplankton community which in turn modify photosynthetic rates of the different size fractions (Poulton et al., 2006).

The majority of the Atlantic Meridional Transect cruises took place during boreal autumn in the Northern hemisphere and austral spring in the Southern hemisphere, and therefore only provided a snap shot of the intra-annual variability in PP. During these times of the year, the NATL and SATL remain strongly stratified which constrains micro-phytoplankton PP (Fig. 2, 3). The Atlantic Gyres remain stratified for most of the year but there are periods, during January in the Northern Hemisphere and July in the Southern Hemisphere (Aiken et al. this issue), when the mixing in these regions can become deeper which could potentially enhance PP, especially micro-phytoplankton PP. From the *in situ* data, the micro-phytoplankton PP varied from 37 mg C m^{-2} d^{-1} in the NATL to 409 mg C m^{-2} d^{-1} in the SSTC and constituted between 18 and 38 % of the total PP. Of the 23 AMT cruises conducted from 1995 to 2013, only 10 cruises (AMT 2-6, 18, 20-23) measured micro-phytoplankton PP. During AMT 2-6, micro-phytoplankton PP was measured using 20 μm

426 polycarbonate filters (Table 1) and these cruises sampled the eastern edge of the NATL, the
427 western edge of the SATL and the CNRY and ETRA (Fig. 1). Three out of five of the cruises
428 were conducted in boreal spring and the other two were during boreal autumn (Table 1).
429 During AMT12-16, the focus on size fractionated PP was in the pico- and nano+micro-
430 phytoplankton (Table 1). During AMT 18, 20-23 10 μm filters were used for micro-
431 phytoplankton PP (Table 1). One may therefore expect that the patterns in size fractionated P_z
432 and PP between AMT 2-6 and AMT18, 20-23 reflect the different pore sized filters used
433 between cruises. This is more constrained, however, by the location of the ship's tracks in the
434 NATL and SATL and the timing of the cruises. During repeat cruises along similar tracks in
435 boreal autumn and using the same pore size (10 μm) for micro-phytoplankton, data from
436 AMT18-23 consistently showed that micro-phytoplankton contribute ~19 % of the total PP in
437 the Atlantic Ocean and at specific depths this reached 38 %. In much of the oligotrophic
438 Atlantic Ocean, the strong vertical stratification of the water column limits the supply of
439 nutrients from below the thermocline to the euphotic layer, thus possibly limiting PP
440 (Maranon et al., 2003) especially in the micro- and nano-phytoplankton size fractions
441 (Aldridge, Purdie & Zubkov, 2014). This may partially explain why micro-phytoplankton PP
442 did not exceed 20 % in these regions. It is not possible to capture all seasons of the year based
443 on *in situ* data alone, but using a satellite model that has been calibrated with representative
444 *PE* parameters, accurate estimates of size-fractionated PP are achievable (Fig. 7; see also
445 Brewin et al. this issue). Such satellite models can then be used to assess intra-, inter- and
446 annual changes in the carbon fixation by different size classes. From the satellite model, the
447 average annual micro-phytoplankton production for the NADR from 1998 to 2010 was 56 g
448 C m^{-2} y^{-1}, in the NATL it was 34 g C m^{-2} y^{-1}, in the WTRA it was 53 g C m^{-2} y^{-1}, 74 g C m^{-2}
449 y^{-1} in the ETRA, for the SATL it was 21 g C m^{-2} y^{-1} and for SSTC region it was 41 g C m^{-2} y^{-1}.
450

451

452 *4.2. Variability in size-fractionated photosynthesis-irradiance parameters.*

453 *4.2.1. Photosynthetic efficiency of size classes.*

454 The determination of size fractionated *PE* curves has been conducted in the global
455 ocean since the 1980's (Joint & Pomroy, 1983; Platt, Rao & Irwin, 1983). The consensus that
456 has emerged is that micro-phytoplankton has the highest P_m^B in open ocean areas of the
457 equatorial tropical and sub-tropical Atlantic and Pacific Oceans (Claustre, Babin, Merien,
458 Ras, Prieur et al., 2005; Li, Karl, Letelier & Church, 2011; Uitz, Huot, Bruyant, Babin &
459 Claustre, 2008), in upwelling of the Canary Current (Cermeno, Maranon, Rodriguez &
460 Fernandez, 2005), especially when diatoms dominate the phytoplankton community (Babin,
461 Morel, Claustre, Bricaud, Kolber et al., 1996; Lorenzo, Arbones, Tilstone & Figueiras, 2005).
462 In upwelling zones this is due to the availability and acquisition of replete light and nutrients
463 by the micro-phytoplankton. In the open ocean, the high photosynthetic rates are associated
464 with filamentous and colonial cyanobacteria and protists (Li et al., 2011), which have the
465 ability to change the number of available photosynthetic reaction centres and can fix nitrogen
466 from the atmosphere suggesting that photosynthesis does not become limited by nutrients (at
467 least by nitrogen). A number of other studies have reported that larger phytoplankton sustain
468 higher biomass-normalised photosynthetic rates than smaller cells due to a higher light
469 utilisation efficiency (Tamigneaux, Legendre, Klein & Mingelbier, 1999). This may in part,
470 be due to their ability to increase the intra-cellular pigment concentrations in response to
471 decreasing growth irradiance (Taylor, Geider & Gilbert, 1997). Though large cells are less
472 efficient at absorbing light due to the package effect, some diatoms have the ability to store
473 nutrients in vacuoles, allowing them to maximise P_m^B during favourable light conditions
474 (Raven, 1997) and some of them have a thick layer of chloroplasts close to the cytoplasm

membrane, which allows the cell surface to maximise the absorption of light. In laboratory based studies, P_m^B of diatoms vary from 1.2 to 11.4 mg C (mg Chl *a*)$^{-1}$ h^{-1} with a mean value of 2.6 ± 1.0. This is similar to the median P_m^B that we measured for micro-phytoplankton in the Atlantic Ocean (~2.88 mg C (mg Chl *a*)$^{-1}$ h^{-1}; Table 4), even though it is difficult to simulate the light field of the natural environment under laboratory conditions. In our study, the range in micro- α^B was from 0.002 mg C (mg Chl-*a*) $^{-1}$ h $^{-1}$ (µmol photons m $^{-2}$ s $^{-1}$) $^{-1}$ in the SATL to 0.085 mg C (mg Chl-*a*) $^{-1}$ h $^{-1}$ (µmol photons m $^{-2}$ s $^{-1}$) $^{-1}$ in the WTRA with an average of 0.013 mg C (mg Chl-*a*) $^{-1}$ h $^{-1}$ (µmol photons m $^{-2}$ s $^{-1}$) $^{-1}$ over the entire Atlantic Ocean. Studies on diatoms have reported a higher range in α^B **,** from 0.013 to 0.087 mg C (mg Chl-*a*) $^{-1}$ h $^{-1}$ (µmol photons m $^{-2}$ s $^{-1}$) $^{-1}$, with an average of 0.021 ± 0.005 mg C (mg Chl-*a*) $^{-1}$ h $^{-1}$ (µmol photons m $^{-2}$ s $^{-1}$) $^{-1}$ (Sarthou et al., 2005). Similarly we found that E_k varied from 6 to 1800 with an average of 420 µmol photons m $^{-2}$ s $^{-1}$ during two AMT cruises in the micro-phytoplankton, whereas for diatoms E_k is reported to be lower, from 46 and 498 µmol photons m $^{-2}$ s $^{-1}$, with an average value of 95 ± 120 µmol photons m $^{-2}$ s $^{-1}$. The higher P_m^B and E_k in the micro-phytoplankton may be the consequence of the very low Chl *a* values associated with these fractions rather than reflecting a higher efficiency of photosynthesis per unit Chl *a*, *per se* (deMadariaga & Joint, 1994). When Chl *a* is close to the analytical detection limit, normalization of photosynthetic rates to Chl *a* can result in inaccuracies, which may not reflect the true photo-physiological response of the phytoplankton community to changes environmental conditions.

To the best of our knowledge our AMT dataset of size fractionated *PE* parameters is the most comprehensive for the Atlantic Ocean to date. We found that from the NADR to the SSTC the average P_m^B for micro-phytoplankton was 4.54 mg C (mg Chl-*a*)$^{-1}$ h^{-1} and for α^B was 0.013 mg C (mg Chl-*a*) $^{-1}$ h $^{-1}$ (µmol photons m $^{-2}$ s $^{-1}$) $^{-1}$, and for P_m^B corresponds to the values reported by Uitz et al. (2008) for the sub-tropical Atlantic, the equatorial Pacific and

500 the Mediterranean Sea and by Barnes, Tilstone, Smyth, Suggett, Astoreca et al. (2014) for the
501 Western English Channel. The micro-phytoplankton mean α^B is similar to that reported by
502 Tilstone, Figueiras, Fermin and Arbones (1999) and Figueiras, Espinoza-Gonzalez, Arbones,
503 Garrido, Teixeira et al. (2014) for the NW Iberian Upwelling system, by Toon, Lohrenz,
504 Rathbun, Wood, Arnone et al. (2000) for the Northern Arabian Sea and by deMadariaga and
505 Joint (1994) for the North Sea. This may suggest that for micro-phytoplankton at least, a
506 common algorithm for the oligotrophic, upwelling shelf and coastal regions of the Atlantic
507 Ocean may be achievable.
508
509 *4.2.2. Depth dependency in photosynthetic parameters of different size-classes.*
510 From the AMT data, $P_m{}^B$ tended to decrease with depth in all size fractions and especially in
511 the NATL, SATL, SSTC, (Fig. 5, 6, Table 3) as a result of moving from high saturating
512 irradiance at the surface to lower irradiance at depth. Similarly, there was a reduction in E_k
513 between the surface and DCM in all size fractions, indicative of photo-acclimation to
514 attenuated light over the water column (Falkowski, 1980). By contrast, α^B values for all size
515 fractions and all provinces were more homogeneous except in the WTRA, with a slight
516 tendency to increase over depth during AMT23 (Fig. 6), reflecting an adaptation to the light
517 environment under stratified conditions. In the WTRA, under the influence of equatorial
518 upwelling and vertical mixing (Fig. 2), α^B values were similar between the surface and DCM
519 for the micro-phytoplankton. Nano-phytoplankton α^B decreased with depth whereas values
520 for pico-phytoplankton increased over depth indicating pico- out compete nano-
521 phytoplankton in light absorption at depth. Similarly Moran and Sharek (2015) found higher
522 α^B in the pico-phytoplankton at depth during summer stratification and little difference in
523 micro-phytoplankton α^B between the surface and deeper in the water column. Such depth
524 dependent patterns in $P_m{}^B$, α^B and E_k have also been reported during stratified conditions in

525 the NW Iberian upwelling zone (Figueiras et al., 2014), the Bay of Biscay (Moran, 2007;
526 Moran & Sharek, 2015) and the North Pacific Gyre (Li et al., 2011), possibly reflecting light
527 acclimation through changes in the number of photosynthetic reaction centres (Behrenfeld,
528 Prasil, Babin & Bruyant, 2004), rather than increases in the size of the light harvesting
529 antennae (Geider, MacIntyre & Kana, 1998). Often an increase in photosynthetic rates has
530 been explained by a decrease in light-harvesting pigment content, which reduces the package
531 effect and enables a more efficient carbon fixation per unit Chl *a* (Berner, Dubinsky, Wyman
532 & Falkowski, 1989). The higher photosynthetic rates that we measured in the micro- and
533 nano-phytoplankton, compared to the pico-phytoplankton, contradicts the theory that small
534 cells are more efficient at light harvesting (Raven, 1998; Veldhuis et al., 2005). This may be
535 partially explained by the fact that the pico-phytoplankton fix a higher percentage of carbon
536 at depth in the water column, whereas micro-phytoplankton fix more carbon closer to the
537 surface. In other studies in the Atlantic Ocean, nano- and micro-phytoplankton consistently
538 showed higher carbon fixation rates than the pico-phytoplankton (Poulton et al., 2006).
539

540 *4.3. Temporal trends in micro-phytoplankton primary production.*

541 Satellite models of size fractionated PP have been developed either based on deriving
542 size fractionated biomass (Uitz et al., 2008) or size fractionated phytoplankton absorption
543 coefficients (Hirata, Hardman-Mountford, Barlow, Lamont, Brewin et al., 2009). Uitz et al.
544 (2008) developed an empirical model of size-fractionated PP based on a large *in situ* data
545 base of phytoplankton pigments, a_{ph}* and *PE* curves taken along latitudinal transects in the
546 sub-tropical Atlantic and Pacific Oceans. This model describes the dependence of algal
547 photo-physiology on phytoplankton size and the relative irradiance of the water column. It
548 has been applied to global ocean colour satellite data to derive PP in micro-, nano- and pico-

549 phytoplankton (Uitz, Claustre, Gentili & Stramski, 2010). In the model, micro-phytoplankton
550 has higher photosynthetic efficiency than the other size classes.

551 In the Atlantic Ocean, Uitz et al. (2010) reported 500 mg C m^{-2} d^{-1} for micro-
552 phytoplankton in the oligotrophic gyres and 1000 mg C m^{-2} d^{-1} along the shelf of the east
553 African upwelling system, with micro-phytoplankton accounting for 15 and 30% of the total
554 PP, respectively. We parameterised a size-fractionated PP model specifically for the Atlantic
555 Ocean and for the oligotrophic gyres. From this model, micro-phytoplankton PP was lower
556 than the estimates given in Uitz et al. (2010) even though similar to our data, Uitz et al.
557 (2008) described micro- P_m^B > nano- P_m^B > pico- P_m^B. In their study, mean P_m^B for micro-,
558 nano- and pico-phytoplankton were 4.26, 2.94 and 3.75 mg C (mg Chl-*a*)$^{-1}$ h^{-1}, respectively,
559 whereas in our study though micro- was similar (4.54 mg C (mg Chl-*a*)$^{-1}$ h^{-1}), nano- P_m^B was
560 higher (4.15 mg C (mg Chl-*a*)$^{-1}$ h^{-1}) and pico-phytoplankton P_m^B was lower (~2.29 mg C (mg
561 Chl-*a*)$^{-1}$ h^{-1}). For α^B Uitz et al. (2008) reported micro- α^B > nano- α^B > pico- α^B in surface
562 waters and nano- α^B > pico- α^B > micro- α^B at depth, with mean α^B of 0.032 mg C (mg Chl-*a*)
563 $^{-1}$ h $^{-1}$ (µmol photons m $^{-2}$ s $^{-1}$) $^{-1}$ for micro-, 0.026 mg C (mg Chl-*a*) $^{-1}$ h $^{-1}$ (µmol photons m $^{-2}$
564 s $^{-1}$) $^{-1}$ for nano-, and 0.007 mg C (mg Chl-*a*) $^{-1}$ h $^{-1}$ (µmol photons m $^{-2}$ s $^{-1}$) $^{-1}$ for pico- over
565 the euphotic zone. By contrast, we found that pico- α^B > micro- α^B > nano- α^B at the surface,
566 and at the DCM this relationship changed by province, reflecting the light acclimation at
567 depth by the different size fractions. Over the entire water column our mean values were
568 lower, with micro- α^B having 0.012 mg C (mg Chl-*a*) $^{-1}$ h $^{-1}$ (µmol photons m $^{-2}$ s $^{-1}$) $^{-1}$, nano-
569 α^B 0.012 mg C (mg Chl-*a*) $^{-1}$ h $^{-1}$ (µmol photons m $^{-2}$ s $^{-1}$) $^{-1}$ and pico- α^B 0.014 mg C (mg Chl-
570 *a*) $^{-1}$ h $^{-1}$ (µmol photons m $^{-2}$ s $^{-1}$) $^{-1}$. The differences in micro-phytoplankton PP between our
571 and the Uitz et al. (2008) are therefore partly due to the representative mean α^B values used,
572 but also since deriving size fractionated Chl *a* from HPLC diagnostic pigments results in
573 higher values compared to sequential filtration through different pore size filters (Brewin,

574 Sathyendranath, Lange & Tilstone, 2014). By Comparison, Figueiras et al. (2014) applied
575 the Uitz et al. (2008) model to the NW Iberian upwelling region and found that it over-
576 estimates size-fractionated PP compared to measured parameters, particularly during periods
577 of upwelling when the water column is mixed, dominated by diatoms and when there is little
578 variation in the *PE* parameters over depth. They concluded that the Uitz et al. (2008) model
579 can only be accurately used for oligotrophic environments where photo-acclimation is a
580 characteristic feature of these highly stratified waters. Global models that assume higher
581 photosynthetic efficiency in a single size class without considering regional variability, may
582 therefore lead to erroneous estimates of size fractionated PP.

583 When we applied our model to SeaWiFS data, we found that micro-phytoplankton PP
584 was constant in most provinces from 1998-2011, except in the BENG and SSTC where it
585 increased significantly over this time period. Similarly, Agirbas, Martinez-Vincente, Brewin,
586 Racault, Airs et al. (2015) observed that Chl *a* measured by HPLC was found to increase in
587 the SATL during boreal autumn from 2003 to 2010. Hirata et al. (2009) used an IOP
588 inversion model to estimate a_{ph} and portioned this between micro-, nano- and pico-
589 phytoplankton using known slopes in these spectra between blue and green wave bands. They
590 then regressed a_{ph} for each size class against size-fractionated PP from simulated *in situ* deck
591 incubations and applied these relationships to satellite data from different upwelling zones. In
592 the BENG and CNRY from 1998 to 2008, Hirata et al. (2009) showed that there was no
593 change in micro-phytoplankton PP over this period. The P_z values that they report for the
594 BENG and CNRY (~0.28 g C m^{-3} d^{-1}) are similar to the values we measured in these
595 provinces (Fig. 3), but in the BENG we observed a slight increase in micro-phytoplankton
596 PP. These differences may be due to the way that the Hirata et al. (2009) model is
597 parameterised based on diagnostic pigments which cannot differentiate for micro-

598 phytoplankton from nano-flagellates such as Phaeocystis spp. which also possess
599 fucoxanthin, the marker pigment for diatoms.

600

601 *4.4. The potential for micro-phytoplankton export production in the Atlantic Ocean.*

602 *4.4.1. Mechanisms for export production.*

603 Early studies on carbon export in the ocean hypothesized that there was a direct link between
604 particulate ExP and PP (Eppley & Peterson, 1979) and that the magnitude of the export is
605 governed by the supply of nutrients into the euphotic zone, the composition and seasonality
606 of primary producers and grazers (Laws, Falkowski, Smith, Ducklow & McCarthy, 2000) and
607 mechanisms of aggregation which make particles sink faster. As aggregated particles sink
608 from the upper mesopelagic zone, they become converted into small, non-sinking POC
609 detritus, which is rapidly metabolized by zooplankton, protozoan and bacterial processes
610 (Belcher et al. 2016). There are three main processes by which phytoplankton are exported to
611 the deep ocean: The first and by far the most important, is through ingestion and excretion by
612 zooplankton (Honjo, Manganini, Krishfield & Francois, 2008). The second mechanism is by
613 gravitational settling of phytoplankton aggregates ballasted by heavy bio-mineral or aerosol
614 lithogenic particles (Armstrong, Lee, Hedges, Honjo & Wakeham, 2002; Francois, Honjo,
615 Krishfield & Manganini, 2002) and the third is through the aggregation of 'heavy'
616 phytoplankton which in turn is modified by bacterial decomposition (e.g. Buesseler,
617 Lamborg, Boyd, Lam, Trull et al., 2007).

618 In productive ecosystems, micro-phytoplankton blooms, especially those dominated
619 by diatoms, are known to trigger substantial export of fast-sinking phyto-detrital aggregates
620 that can carpet the deep ocean floor (Honjo & Manganini, 1993). There are a number of
621 hypotheses to explain this mechanism: 1.) silicate limitation of diatoms at the end of a bloom
622 can lead to transparent exo-polymer particles (TEP) being formed (Sieracki, Verity &

623 Stoecker, 1993), which causes cells to stick together promoting aggregation, sinking and
624 sedimentation (Kiørboe, Hansen, Alldredge, Jackson, Passow et al., 1996); 2.) higher inputs
625 of nutrients as a result of deep mixed layers or upwelling lead to enhanced PP that favours
626 micro-phytoplankton which augments the export of siliceous particulate organic matter (Brix,
627 Gruber, Karl & Bates, 2006); 3.) Low temperatures cause a slow-down in heterotrophic
628 processes compared to autotrophic processes, which can subsequently lead to the
629 intensification of ExP (Laws et al., 2000). On 1.), the silicate content of diatoms can be a
630 function of growth rate (Claquin et al., 2002), which may cause nitrate and phosphorus
631 limitation that may enhance sedimentation rates. By comparison, silicate limitation can cause
632 low silicate frustule content, which could reduce sinking rates.
633
634 *4.4.2. Export production in the Atlantic Ocean.*
635 There are a wide variety of techniques to measure ExP with increasing interest in the
636 use of radionuclide disequilibria technique between thorium-234 (^{234}Th) and its parent
637 uranium-238 (^{238}U) as a tracer of particle export, has resulted in a comprehensive global data
638 base of ThExP (Le Moigne, Henson, Sanders & Madsen, 2013). In this study we were able to
639 address the question: How do the estimates of ThExP that we computed using the algorithm
640 of Henson et al. (2011), compare with those reported in other studies? The ^{234}Th technique
641 was deployed during AMT14 in 2004 to measure POC export in Atlantic Ocean Provinces
642 (Thomalla, Turnewitsch, Lucas & Poulton, 2006). The lowest ^{234}Th-derived POC export
643 fluxes were in the Atlantic Gyres with 0 g C m^{-2} d^{-1} measured in the NATL and 0.07 g C m^{-2}
644 d^{-1} in the SATL, where ExP was between < 10 and 246 % of total PP. By contrast, higher
645 export flux was associated with the equatorial upwelling regions of the ETRA (0.30 g C m^{-2}
646 d^{-1}) and WTRA (0.18 g C m^{-2} d^{-1}) and also in the NADR and SSTC (0.08 – 0.49 g C m^{-2} d^{-1}),
647 which was 20 – 50 % of total PP. By comparison, using total PP from SeaWiFS during April

& May 2004, we estimate an average ThExP of 0.017 and 0.010 g C m^{-2} d^{-1} in the NATL and SATL; 0.018 and 0.014 g C m^{-2} d^{-1} in the ETRA and WTRA and 0.058 and 0.029 g C m^{-2} d^{-1} in the NADR and SSTC, respectively. Similarly using total PP from the SeaWiFS time series (1998-2010) we estimate an average ThExP of 0.013 and 0.011 g C m^{-2} d^{-1} in the NATL and SATL; 0.023 and 0.015 g C m^{-2} d^{-1} in the ETRA and WTRA and 0.044 and 0.036 g C m^{-2} d^{-1} in the NADR and SSTC. The values we compute were slightly lower than those given in Thomalla et al. (2006) since we estimated average values over each province whereas Thomalla et al. (2006) measured ThExP at point stations.

4.4.3. The potential contribution of micro-phytoplankton to export production.

It has been observed in many oligotrophic environments that micro-phytoplankton, and especially the diatoms, contribute more to ExP than to PP (Goldman & McGillicuddy, 2003; Karl, Michaels, Bergman, Capone, Carpenter et al., 2002). Diatoms alone account for 9–20% of organic carbon export in the North Pacific Subtropical Gyre (Brzezinski , Krause, Church, Karl, Li et al., 2011), 15–20% of the ExP in the equatorial Pacific (Krause, Nelson & Brzezinski, 2011) and up to 30% in the Sargasso Sea at BATS (Nelson & Brzezinski, 1997). At BATS positive correlations between temperature and export ratios, and between wind speed and total PP, suggests that total PP increases when MLD is at its maximum and nutrient supply at its peak, and that ExP increases afterwards with the onset of stratification and increases in temperature (Brix et al. 2006). These changes in mixing and nutrient supply and also in light intensity produce a shift in phytoplankton community from pico-phytoplankton to larger phytoplankton which is also correlated with the export flux (Casey, Aucan, Goldberg & Lomas, 2013). Considering the magnitude of micro-phytoplankton PP, we found that SSTC is the most efficient export system (ThExP / micro-PP ratio ~0.44) and the ETRA is the least efficient (ThExP / micro-PP ratio ~0.07). The upwelling regions of the

673 CNRY and BENG and the NADR have a ThExP / micro-PP ratio of ~0.2 and the NATL,
674 SATL and WTRA are closer to 0.1.
675
676 **5. Conclusions.**
677 A large *in situ* database from the Atlantic Meridional Transect of micro-phytoplankton P_z, PP
678 and *PE* parameters was used to quantify the contribution of micro-phytoplankton to total PP
679 in different Atlantic Provinces. For cruises that sampled the edge of the NATL the % micro-
680 phytoplankton P_z to total P_z in the top 50 m was ~30% in the NADR and NATL, but
681 decreased to 15 - 30 % in the WTRA and SATL. On cruises that sampled closer to the centre
682 of the NATL, % micro-P_z was <15 %, reaching ~20 % at the boundaries between the NATL,
683 SATL and WTRA. We found that over the Atlantic basin, micro-phytoplankton had the
684 highest P_m^B (~5 mg C (mg Chl *a*)$^{-1}$ h^{-1}), followed by nano- (~4 mg C (mg Chl *a*)$^{-1}$ h^{-1}) and
685 pico-phytoplankton (~2 mg C (mg Chl *a*)$^{-1}$ h^{-1}). The highest micro-phytoplankton P_m^B was in
686 the NATL and the lowest values were in the NADR and SATL. The *PE* parameters were
687 used to calibrate a remote sensing model of micro-phytoplankton PP, which were within 14
688 % of *in situ* values. When the model was applied to the SeaWiFS time series, it revealed that
689 that micro-phytoplankton PP remained fairly constant from 1998 to 2010 in the NADR,
690 NATL, CNRY, ETRA, WTRA and SATL, but showed a gradual increase in the BENG and
691 SSTC. We also used the algorithm of Henson et al. (2011) to estimate ThExP from total PP
692 and compared this with micro-phytoplankton PP. The results suggest that micro-
693 phytoplankton PP in the SSTC potentially export 44 % of their production, whereas in the
694 NATL, SATL and WTRA micro-phytoplankton only account for 10 % of the ThExP.
695
696 **Acknowledgements.**

We would like to thank the captain and crews of *RRS Discovery*, *RRS James Cook* and *RRS James Clark Ross* on AMT1-23. We would also like to thank the Natural Environment Research Council (NERC) Earth Observation Data Acquisition and Analysis Service (NEODAAS) for their role in processing satellite imagery and use of their Linux cluster for running the satellite model. This study is a contribution to the international IMBER project and was supported by the UK Natural Environment Research Council National Capability funding to Plymouth Marine Laboratory and the National Oceanography Centre, Southampton. PKL and AM on AMT22 and 23 respectively, were supported by POGO fellowships and the EU FP7 project GreenSeas (no. 265294). RJWB was supported by NCEO. This is contribution number 279 of the AMT programme.

References

Agirbas, E., Martinez-Vincente, V., Brewin, R.J.W., Racault, M.-F., Airs, R.L., Llewellyn, C.A., 2015. Temporal changes in total and size-fractioned chlorophyll-a in surface waters of three provinces in the Atlantic Ocean (September to November) between 2003 and 2010. . *Journal of Marine Systems*, 150, 56-65.

Aldridge, D., Purdie, D.A., Zubkov, M.V., 2014. Growth and survival of neoceratium hexacanthum and neoceratium candelabrum under simulated nutrient-depleted conditions. *Journal of Plankton Research*, 36, 439-449.

Armstrong, R., Lee, C., Hedges, J., Honjo, S., Wakeham, S., 2002. A new, mechanistic model for organic carbon fluxes in the ocean based on the quantitative association of POC with ballast minerals. *Deep-Sea Research II*, 49, 219–236.

Azam, F., 1998. Microbial control of oceanic carbon flux: The plot thickens. *Science*, 280, 694-696.

Babin, M., Morel, A., Claustre, H., Bricaud, A., Kolber, Z., Falkowski, P.G., 1996. Nitrogen- and irradiance-dependent variations of the maximum quantum yield of carbon fixation in eutrophic, mesotrophic and oligotrophic marine systems. *Deep-Sea Research Part I-Oceanographic Research Papers*, 43, 1241-1272.

Barlow, R.G., Aiken, J., Holligan, P.M., Cummings, D.G., Maritorena, S., Hooker, S., 2002. Phytoplankton pigment and absorption characteristics along meridional transects in the Atlantic Ocean. *Deep-Sea Research Part I-Oceanographic Research Papers*, 49, 637-660.

Barlow, R.G., Aiken, J., Moore, G.F., Holligan, P.M., Lavender, S., 2004. Pigment adaptations in surface phytoplankton along the eastern boundary of the Atlantic Ocean. *Marine Ecology-Progress Series*, 281, 13-26.

731 Barnes, M.K., Tilstone, G.H., Smyth, T.J., Suggett, D.J., Astoreca, R., Lancelot, C.,
732 Kromkamp, J.C., 2014. Absorption-based algorithm of primary production for total and size-
733 fractionated phytoplankton in coastal waters. *Marine Ecology Progress Series*, 504, 1-12.
734 Beardall, J., Raven, J.A., 2004. The potential effects of global climate change on microalgal
735 photosynthesis, growth and ecology. *Phycologia*, 43, 26-40.
736 Behrenfeld, M.J., Prasil, O., Babin, M., Bruyant, F., 2004. In search of a physiological basis
737 for covariations in light- limited and light-saturated photosynthesis. *Journal of Phycology*, 40,
738 4-25.
739 Belcher, A., Iversen, M., Giering, S., Riou, V., Henson, S. A., Berline, L., Guilloux, L.,
740 Sanders, R. 2016. Depth-resolved particle-associated microbial respiration in the northeast
741 Atlantic. *Biogeosciences*, 13: 4927-4943.
742 Bell, T., Kalff, J., 2001. The contribution of picophytoplankton in marine and freshwater
743 systems of different trophic status and depth. *Limnology and Oceanography*, 46, 1243-1248.
744 Berner, T., Dubinsky, Z., Wyman, K., Falkowski, P.G., 1989. Photoadaptation and the
745 package effect in Dunaliella-tertiolecta (Chlorophyceae). *Journal of Phycology*, 25, 70-78.
746 Bienfang, P.K., 1981. SETCOL - A technologically simple and reliable method for
747 measuring phytoplankton sinking rates. *Canadian Journal of Fisheries and Aquatic Sciences*,
748 38, 1289-1294.
749 Biller, S.J., Berube, P.M., Lindell, D., Chisholm, S.W., 2015. Prochlorococcus: The structure
750 and function of collective diversity. *Nature Reviews Microbiology*, 13, 13-27.
751 Brewin, R.J.W., Sathyendranath, S., Lange, P.K., Tilstone, G., 2014. Comparison of two
752 methods to derive the size-structure of natural populations of phytoplankton. . *Deep-Sea*
753 *Research I*, 85, 72-79.
754 Brewin, R.J.W., Sathyendranath, S., Tilstone, G., Lange, P.K., Platt, T., 2014. A
755 multicomponent model of phytoplankton size structure. *Journal of Geophysical Research-*
756 *Oceans*, 119, 3478-3496.
757 Brix, H., Gruber, N., Karl, D.M., Bates, N.R., 2006. On the relationships between primary,
758 net community, and export production in subtropical gyres. *Deep-Sea Research II*, 53, 698–
759 717.
760 Brzezinski , M.A., Krause, J.W., Church, M.J., Karl, D.M., Li, B., Jones, J.L., Updyke, B.,
761 2011. The annual silica cycle of the North Pacific subtropical gyre. *Deep-Sea Research I*, 58,
762 988–1001.
763 Buesseler, K.O., Lamborg, C.H., Boyd, P.W., Lam, P.L., Trull, T.W., Bidigare, R.R., Bishop,
764 J.K.B., Casciotti, K.L., Dehairs, F., Elskens, M., Honda, M., Karl, D.M., Siegel, D.A., Silver,
765 M.W., Steinberg, D.K., Valdes, J., Van Mooy, B., Wilson, S., 2007. Revisiting carbon flux
766 through the ocean's ''twilight zone". . *Science*, 316, 567–570.
767 Campbell, J., Antoine, D., Armstrong, R., Arrigo, K., Balch, W., Barber, R., Behrenfeld, M.,
768 Bidigare, R., Bishop, J., Carr, M.E., Esaias, W., Falkowski, P., Hoepffner, N., Iverson, R.,
769 Kiefer, D., Lohrenz, S., Marra, J., Morel, A., Ryan, J., Vedernikov, V., Waters, K., Yentsch,
770 C., Yoder, J., 2002. Comparison of algorithms for estimating ocean primary production from
771 surface chlorophyll, temperature, and irradiance. *Global Biogeochemical Cycles*, 16, art. no.-
772 1035.
773 Carr, M.E., Friedrichs, M.A.M., Schmeltz, M., Aita, M.N., Antoine, D., Arrigo, K.R.,
774 Asanuma, I., Aumont, O., Barber, R., Behrenfeld, M., Bidigare, R., Buitenhuis, E.T.,
775 Campbell, J., Ciotti, A., Dierssen, H., Dowell, M., Dunne, J., Esaias, W., Gentili, B., Gregg,
776 W., Groom, S., Hoepffner, N., Ishizaka, J., Kameda, T., Le Quere, C., Lohrenz, S., Marra, J.,
777 Melin, F., Moore, K., Morel, A., Reddy, T.E., Ryan, J., Scardi, M., Smyth, T., Turpie, K.,
778 Tilstone, G., Waters, K., Yamanaka, Y., 2006. A comparison of global estimates of marine
779 primary production from ocean color. *Deep-Sea Research Part Ii-Topical Studies in*
780 *Oceanography*, 53, 741-770.

781 Casey, J.R., Aucan, J.P., Goldberg, S.R., Lomas, M.W., 2013. Changes in partitioning of
782 carbon amongst photosynthetic pico- and nano-plankton groups in the Sargasso Sea in
783 response to changes in the North Atlantic Oscillation. *Deep-Sea Research II*, 93, 58–70.
784 Cermeno, P., Maranon, E., Rodriguez, J., Fernandez, E., 2005. Large-sized phytoplankton
785 sustain higher carbonspecific photosynthesis than smaller cells in a coastal eutrophic
786 ecosystem. *Marine Ecology-Progress Series*, 297, 51-60.
787 Chisholm, S.W., 1992. *Phytoplankton Size.*
788 Cho, B.C., Azam, F., 1988. Major role of bacteria in biogeochemical fluxes in the oceans
789 interior. *Nature*, 332, 441-443.
790 Claquin, P., Martin-Jezequel, V., Kromkamp, J. C., Veldhuis, M. J. W., Kraay, G. W. 2002.
791 Uncoupling of silicon compared with carbon and nitrogen metabolisms and the role of the
792 cell cycle in continuous cultures of Thalassiosira pseudonana (Bacillariophyceae) under light,
793 nitrogen, and phosphorus control. *Journal of Phycology*, 38: 922-930.
794 Claustre, H., Babin, M., Merien, D., Ras, J., Prieur, L., Dallot, S., 2005. Toward a
795 taxonspecific parameterization of bio-optical models of primary production: a case study in
796 the North Atlantic. *Journal of Geophysical Research C: Oceans*, 110.
797 Cushing, D.H., 1989. A difference in structure between ecosystems in strongly stratified
798 waters and in those that are only weakly stratified. *Journal of Plankton Research*, 11, 1-13.
799 deMadariaga, I., Joint, I.R., 1994. Photosynthesis and carbon metabolism by size-fractionated
800 phytoplankton in the southern North Sea in early summer. *Continental Shelf Research*, 14,
801 295-311.
802 Dodge, J.D., Marshall, H.G., 1994. Biogeographic analysis of the armored planktonic
803 dinoflagellate Ceratium in the North-Atlantic and adjacent seas. *Journal of Phycology*, 30,
804 905-922.
805 Dugdale, R.C., Goering, J.J., 1967. Uptake of new and regenerated forms of nitrogen in
806 primary productivity. *Limnology and Oceanography.*, 12, 196-206.
807 Eppley, R.W., Peterson, B.J., 1979. Particulate Organic-Matter Flux and Planktonic New
808 Production in the Deep Ocean. *Nature*, 282, 677-680.
809 Falkowski, P.G., Barber, R.T., Smetacek, V., 1998. Biogeochemical controls and feedbacks
810 on ocean primary production. *Science*, 281, 200-206.
811 Figueiras, F.G., Espinoza-Gonzalez, O., Arbones, B., Garrido, J.L., Teixeira, I.G., Castro,
812 C.G., 2014. Estimating phytoplankton size-fractionated primary production in the
813 northwestern Iberian upwelling: Is mixotrophy relevant in pigmented nanoplankton?
814 *Progress in Oceanography*, 128, 88-97.
815 Francois, R., Honjo, S., Krishfield, R., Manganini, S., 2002. Factors controlling the flux of
816 organic carbon to the bathypelagic zone of the ocean. *Global Biogeochem Cycles*, 16.
817 Friedrichs, M.A.M., Carr, M.-E., Barber, R.T., Scardi, M., Antoine, D., Armstrong, R.A.,
818 Asanuma, I., Behrenfeld, M.J., Buitenhuis, E.T., Chai, F., Christian, J.R., Ciotti, A.M.,
819 Doney, S.C., Dowell, M., Dunne, J., Gentili, B., Gregg, W., Hoepffner, N., Ishizaka, J.,
820 Kameda, T., Lima, I., Marra, J., Melin, F., Moore, J.K., Morel, A., O'Malley, R.T., O'Reilly,
821 J., Saba, V.S., Schmeltz, M., Smyth, T.J., Tjiputra, J., Waters, K., Westberry, T.K., Winguth,
822 A., 2009. Assessing the uncertainties of model estimates of primary productivity in the
823 tropical Pacific Ocean. *Journal of Marine Systems*, 76, 113-133.
824 Geider, R.J., MacIntyre, H.L., Kana, T.M., 1998. A dynamic regulatory model of
825 phytoplanktonic acclimation to light, nutrients, and temperature. *Limnology and*
826 *Oceanography*, 43, 679-694.
827 Gibb, S.W., Barlow, R.G., Cummings, D.G., Rees, N.W., Trees, C.C., Holligan, P., Suggett,
828 D., 2000. Surface phytoplankton pigment distributions in the Atlantic Ocean: an assessment
829 of basin scale variability between 50 degrees N and 50 degrees S. *Progress in Oceanography*,
830 45, 339-368.

Goldman, J.C., McGillicuddy, D.J., 2003. Effect of large marine diatoms growing at low light on episodic new production. *Limnology and Oceanography*, 48, 1176–1182.
Grob, C., Jardillier, L.E., Hartmann, M., Ostrowski, M., Zubkov, M.V., Scanlan, D.J., 2015. Cell-specific CO2 fixation rates of two taxonomically distinct groups of plastidic protists in the Atlantic Ocean remain unchanged after nutrient addition. *Environmental Microbiology Reports*, 7, 211-218.
Grosskopf, T., Mohr, W., Baustian, T., Schunck, H., Gill, D., Kuypers, M.M.M., Lavik, G., Schmitz, R.A., Wallace, D.W.R., LaRoche, J., 2012. Doubling of marine dinitrogen-fixation rates based on direct measurements. *Nature*, 488, 361-364.
Hays, G.C., Richardson, A.J., Robinson, C., 2005. Climate change and marine plankton. *Trends in Ecology & Evolution*, 20, 337-344.
Henson, S.A., Sanders, R., Madsen, E., Morris, P.J., Le Moigne, F., Quartly, G.D., 2011. A reduced estimate of the strength of the ocean's biological carbon pump. *Geophysical Research Letters*, 38.
Hirata, T., Hardman-Mountford, N.J., Barlow, R., Lamont, T., Brewin, R.J.W., Smyth, T., Aiken, J., 2009. An inherent optical property approach to the estimation of size-specific photosynthetic rates in eastern boundary upwelling zones from satellite ocean colour: an initial assessment. . *Progress in Oceanography*, 83, 393–397.
Honjo, S., Manganini, S.J., 1993. Annual biogenic particle fluxes to the interior of the North Atlantic ocean; studied at 34 ⌖N 21 ⌖W and 48 ⌖N 21 ⌖W. . *Deep-Sea Research I*, 40, 587–607.
Honjo, S., Manganini, S.J., Krishfield, R.A., Francois, R., 2008. Particulate organic carbon fluxes to the ocean interior and factors controlling the biological pump: A synthesis of global sediment trap programs since 1983. *Progress in Oceanography*, 76, 217–285.
Jochem, F.J., Zeitzschel, B., 1993. Productivity regime and phytoplankton size structure in the tropical and subtropical North-Atlantic in spring 1989. *Deep-Sea Research Part Ii-Topical Studies in Oceanography*, 40, 495-519.
Joint, I.R., Pomroy, A.J., 1983. Production of picoplankton and small nanoplankton in the Celtic Sea. *Marine Biology*, 77, 19-27.
Karl, D., Michaels, A., Bergman, B., Capone, D., Carpenter, E., Letelier, R., Lipschultz, F., Paerl, H., Sigman, D., Stal, L., 2002. Dinitrogen fixation in the world's oceans. . *Biogeochemistry*, 57, 47–98.
Kiorboe, T., 1993. Turbulence, phytoplankton cell-size, and the structure of pelagic food webs. *Advances in Marine Biology, Vol 29*, 29, 1-72.
Kiørboe, T., Hansen, J.L.S., Alldredge, A.L., Jackson, G.A., Passow, U., Dam, H.G., Drapeau, D.T., Waite, A., Garcia, C.M., 1996. Sedimentation of phytoplankton during a diatom bloom: rates and mechanisms. *Journal of Marine Research*, 54, 1123–1148.
Krause, J.W., Nelson, D.M., Brzezinski, M.A., 2011. Biogenic silica production and diatoms' contribution to primary and new production in the eastern equatorial Pacific. . *Deep-Sea Research II*, 58, 434–448.
Laws, E.A., Falkowski, P.G., Smith, W.O., Ducklow, H., McCarthy, J.J., 2000. Temperature effects on export production in the open ocean. *Global Biogeochemical Cycles*, 14, 1231-1246.
Le Moigne, F.A.C., Henson, S.A., Sanders, R.J., Madsen, E., 2013. Global database of surface ocean particulate organic carbon export fluxes diagnosed from the 234Th technique. . *Earth System Science Data*, 5, 295–304.
Legendre, L., Lefevre, J., 1989. *Hydrodynamical singularities as controls of recycled versus export production in oceans*.

879 Li, B., Karl, D.M., Letelier, R.M., Church, M.J., 2011. Size-dependent photosynthetic
880 variability in the North Pacific Subtropical Gyre. *Marine Ecology Progress Series*, 440, 27-
881 40.
882 Lorenzo, L.M., Arbones, B., Tilstone, G.H., Figueiras, F.G., 2005. Across-shelf variability of
883 phytoplankton composition, photosynthetic parameters and primary production in the NW
884 Iberian upwelling system. *Journal of Marine Systems*, 54, 157-173.
885 Mann, D.G., 1999. The species concept in diatoms. *Phycologia*, 38, 437-495.
886 Maranon, E., Behrenfeld, M.J., Gonzalez, N., Mourino, B., Zubkov, M.V., 2003. High
887 variability of primary production in oligotrophic waters of the Atlantic Ocean: uncoupling
888 from phytoplankton biomass and size structure. *Marine Ecology-Progress Series*, 257, 1-11.
889 Maranon, E., Holligan, P.M., Barciela, R., Gonzalez, N., Mourino, B., Pazo, M.J., Varela, M.,
890 2001. Patterns of phytoplankton size structure and productivity in contrasting open-ocean
891 environments. *Marine Ecology-Progress Series*, 216, 43-56.
892 Maranon, E., Holligan, P.M., Varela, M., Mourino, B., Bale, A.J., 2000. Basin-scale
893 variability of phytoplankton biomass, production and growth in the Atlantic Ocean. *Deep-Sea*
894 *Research Part I-Oceanographic Research Papers*, 47, 825-857.
895 Moran, X.A.G., 2007. Annual cycle of picophytoplankton photosynthesis and growth rates in
896 a temperate coastal ecosystem: a major contribution to carbon fluxes. *Aquatic Microbial*
897 *Ecology*, 49, 267 - 279.
898 Moran, X.A.G., Sharek, R., 2015. Photosynthetic parameters and primary production, with
899 focus on large phytoplankton, in a temperate mid-shelf ecosystem. . *Estuarine, Coastal and*
900 *Shelf Science*, 154, 255-263.
901 Morel, A., 1991. Light and Marine Photosynthesis - a Spectral Model with Geochemical and
902 Climatological Implications. *Progress in Oceanography*, 26, 263-306.
903 Morel, A., Huot, Y., Gentili, B., Werdell, P. J., Hooker, S. B., Franz, B. A. 2007. Examining
904 the consistency of products derived from various ocean color sensors in open ocean (Case 1)
905 waters in the perspective of a multi-sensor approach. *Remote Sensing of Environment*, 111:
906 69-88.
907 Nelson, D.M., Brzezinski, M.A., 1997. Diatom growth and productivity in an oligotrophic
908 midocean gyre: a 3-yr record from the Sargasso Sea near Bermuda. *Limnology and*
909 *Oceanography*, 42, 473–486.
910 Nelson, D.M., Treguer, P., Brzezinski, M.A., Leynaert, A., Queguiner, B., 1995. Production
911 and dissolution of biogenic silica in the ocean - revised global estimates, comparison with
912 regional data and relationship to biogenic sedimentation. *Global Biogeochemical Cycles*, 9,
913 359-372.
914 Olson, E.M., McGillicuddy, D.J., Flierl, G.R., Davis, C.S., Dyhrman, S.T., Waterbury, J.B.,
915 2015. Mesoscale eddies and Trichodesmium spp. distributions in the southwestern North
916 Atlantic. *Journal of Geophysical Research C: Oceans*, 120, 4129-4150.
917 Partensky, F., Hess, E.R., Vaulot, D., 1999. Prochlorococcus, a marine phytosynsynthetic
918 prokaryote of global signifcance. *Microbiol. Mol. Biol. Rev.*, 63, 106-127.
919 Perez, V., Fernandez, E., Maranon, E., Serret, P., Garcia-Soto, C., 2005a. Seasonal and
920 interannual variability of chlorophyll a and primary production in the Equatorial Atlantic: in
921 situ and remote sensing observations. *Journal of Plankton Research*, 27, 189-197.
922 Perez, V., Fernandez, E., Maranon, E., Serret, P., Varela, R., Bode, A., Varela, M., Varela,
923 M.M., Moran, X., Woodward, E.M.S., Kitidis, V., Garcia-Soto, C., 2005b. Latitudinal
924 distribution of microbial plankton abundance, production, and respiration in the Equatorial
925 Atlantic in Autumn 2000. *Deep-Sea Research Part I-Oceanographic Research Papers*, 52,
926 861-880.
927 Platt, T., Gallegos, C.L., Harrison, W.G., 1980. Photoinhibition of photosynthesis in natural
928 assemblages of marine-phytoplankton. *Journal of Marine Research*, 38, 687-701.

929 Platt, T., Rao, D.V.S., Irwin, B., 1983. Photosynthesis of picoplankton in the oligotrophic
930 ocean. *Nature*, 301, 702-704.
931 Platt, T., Sathyendranath, S., 1988. Oceanic Primary Production - Estimation by Remote-
932 Sensing at Local and Regional Scales. *Science*, 241, 1613-1620.
933 Poulton, A.J., Holligan, P.M., Hickman, A., Kim, Y.N., Adey, T.R., Stinchcombe, M.C.,
934 Holeton, C., Root, S., Woodward, E.M.S., 2006. Phytoplankton carbon fixation, chlorophyll-
935 biomass and diagnostic pigments in the Atlantic Ocean. *Deep-Sea Research Part Ii-Topical*
936 *Studies in Oceanography*, 53, 1593-1610.
937 Raven, J.A., 1997. Inorganic carbon acquisition by marine autotrophs. *Advances in Botanical*
938 *Research, Vol 27: Classic Papers*, Vol. 27 (pp. 85-209).
939 Raven, J.A., 1998. The twelfth Tansley Lecture. Small is beautiful: the picophytoplankton.
940 *Functional Ecology*, 12, 503-513.
941 Saba, V.S., Friedrichs, M.A.M., Carr, M.-E., Antoine, D., Armstrong, R.A., Asanuma, I.,
942 Aumont, O., Bates, N.R., Behrenfeld, M.J., Bennington, V., Bopp, L., Bruggeman, J.,
943 Buitenhuis, E.T., Church, M.J., Ciotti, A.M., Doney, S.C., Dowell, M., Dunne, J.,
944 Dutkiewicz, S., Gregg, W., Hoepffner, N., Hyde, K.J.W., Ishizaka, J., Kameda, T., Karl,
945 D.M., Lima, I., Lomas, M.W., Marra, J., McKinley, G.A., Melin, F., Moore, J.K., Morel, A.,
946 O'Reilly, J., Salihoglu, B., Scardi, M., Smyth, T.J., Tang, S., Tjiputra, J., Uitz, J., Vichi, M.,
947 Waters, K., Westberry, T.K., Yool, A., 2010. Challenges of modeling depth-integrated
948 marine primary productivity over multiple decades: A case study at BATS and HOT. *Global*
949 *Biogeochemical Cycles*, 24.
950 Sarthou, G., Timmermans, K.R., Blain, S., Treguer, P., 2005. Growth physiology and fate of
951 diatoms in the ocean: a review. *Journal of Sea Research*, 53, 25-42.
952 Sieracki, M.E., Verity, P.G., Stoecker, D.K., 1993. Plankton community response to
953 sequential silicate and nitrate depletion during the 1989 North Atlantic Spring Bloom. . *Deep-*
954 *Sea Research II*, 40, 213–225.
955 Smetacek, V., 1999. Diatoms and the ocean carbon cycle. *Protist*, 150, 25-32.
956 Smyth, T.J., Tilstone, G.H., Groom, S.B., 2005. Integration of radiative transfer into satellite
957 models of ocean primary production. *Journal of Geophysical Research-Oceans*, 110.
958 Svensen, C., Morata, N., Reigstad, M., 2014. Increased degradation of copepod faecal pellets
959 by co-acting dinoflagellates and Centropages hamatus. *Marine Ecology Progress Series*, 516,
960 61-70.
961 Tamigneaux, E., Legendre, L., Klein, B., Mingelbier, M., 1999. Seasonal dynamics and
962 potential fate of size-fractionated phytoplankton in a temperate nearshore environment
963 (western Gulf of St Lawrence, Canada). *Estuarine, Coastal and Shelf Science*, 48, 253-269.
964 Tarran, G.A., Heywood, J.L., Zubkov, M.V., 2006. Latitudinal changes in the standing stocks
965 of nano- and picoeukaryotic phytoplankton in the Atlantic Ocean. *Deep-Sea Research Part*
966 *Ii-Topical Studies in Oceanography*, 53, 1516-1529.
967 Taylor, A.H., Geider, R.J., Gilbert, F.J.H., 1997. Seasonal and latitudinal dependencies of
968 phytoplankton carbon-to-chlorophyll a ratios: results of a modelling study. *Marine Ecology*
969 *Progress Series*, 152, 51–66.
970 Thomalla, S., Turnewitsch, R., Lucas, M., Poulton, A., 2006. Particulate organic carbon
971 export from the North and South Atlantic gyres: the Th-234 / U-238 disequilibrium approach.
972 . *Deep-Sea Research II*, 53, 1629–1648.
973 Tilstone, G., Smyth, T., Poulton, A., Hutson, R., 2009. Measured and remotely sensed
974 estimates of primary production in the Atlantic Ocean from 1998 to 2005. *Deep-Sea*
975 *Research Part II-Topical Studies in Oceanography*, 56, 918-930.
976 Tilstone, G.H., Figueiras, F.G., Fermin, E.G., Arbones, B., 1999. Significance of
977 nanophytoplankton photosynthesis and primary production in a coastal upwelling system (Ria
978 de Vigo, NW Spain). *Marine Ecology-Progress Series*, 183, 13-27.

Tilstone, G.H., Figueiras, F.G., Lorenzo, L.M., Arbones, B., 2003. Phytoplankton composition, photosynthesis and primary production during different hydrographic conditions at the Northwest Iberian upwelling system (vol 525, pg 89, 2003). *Marine Ecology-Progress Series*, 254, 313-313.

Toon, R.K., Lohrenz, S.E., Rathbun, C.E., Wood, A.M., Arnone, R.A., Jones, B.H., Kindle, J.C., Weidemann, A.D., 2000. Photosynthesis-irradiance parameters and community structure associated with coastal filaments and adjacent waters in the northern Arabian Sea. *Deep-Sea Research II*, 47, 1249-1277.

Treguer, P., Nelson, D.M., Vanbennekom, A.J., Demaster, D.J., Leynaert, A., Queguiner, B., 1995. The silica balance in the world ocean - A reestimate. *Science*, 268, 375-379.

Treguer, P., Pondaven, P., 2000. Global change - Silica control of carbon dioxide. *Nature*, 406, 358-359.

Uitz, J., Claustre, H., Gentili, B., Stramski, D., 2010. Phytoplankton class-specific primary production in the world's oceans: Seasonal and interannual variability from satellite observations. *Global Biogeochemical Cycles*, 24.

Uitz, J., Claustre, H., Morel, A., Hooker, S.B., 2006. Vertical distribution of phytoplankton communities in open ocean: An assessment based on surface chlorophyll. *Journal of Geophysical Research-Oceans*, 111.

Uitz, J., Huot, Y., Bruyant, F., Babin, M., Claustre, H., 2008. Relating phytoplankton photophysiological properties to community structure on large scales. *Limnology and Oceanography*, 53, 614-630.

Veldhuis, M.J.W., Timmermans, K.R., Croot, P., van der Wagt, B., 2005. Picophytoplankton; a comparative study of their biochemical composition and photosynthetic properties. *Journal of Sea Research*, 53, 7-24.

Welschmeyer, N.A., 1994. Fluorometric Analysis of Chlorophyll-a in the Presence of Chlorophyll-B and Pheopigments. *Limnology and Oceanography*, 39, 1985-1992.

Zubkov, M.V., Sleigh, M.A., Burkill, P.H., 2000. Assaying picoplankton distribution by flow cytometry of underway samples collected along a meridional transect across the Atlantic Ocean. *Aquatic Microbial Ecology*, 21, 13-20.

Zubkov, M.V., Sleigh, M.A., Tarran, G.A., Burkill, P.H., Leakey, R.J.G., 1998. Picoplanktonic community structure on an Atlantic transect from 50 degrees N to 50 degrees S. *Deep-Sea Research Part I-Oceanographic Research Papers*, 45, 1339-1355.

Figure Legends.

Figure 1. Station locations: (A.) AMT 1 to AMT 11, (B.) AMT12 to 22, (C.) AMT 22 and 23 and (D.) Longhurst Provinces.

Figure 2. Sections of CTD temperature, salinity and chlorophyll *a* estimated from fluorescence for Boreal Spring (A, B, C) and Boreal Autumn (D, E, F).

Figure 3. Sections of total water integrated primary production (mg C m^{-3} d^{-1}) and mean percentage of microphytoplankton (>10 μm) and picoplankton (0.2-2 μm) primary production during Boreal Spring (A, B, C) and AMT Boreal Autumn (D, E, F).

Figure 4. Integrated primary production (mg C m^{-2} d^{-1}) for (A.) micro-, (B.) nano-, (C.) pico-phytoplankton and percentage of total primary production for (D.) micro-, (E.) nano-, (F.) pico-phytoplankton during AMT 18 to AMT 23.

Figure 5. Size Fractionated Photosynthesis-Irradiance parameters from surface samples on AMT22 (A.) PmB, (B.) alphaB, (C.) Ek and AMT23 (D.) PmB, (E.) alphaB, (F.) Ek. Dark grey bar is micro- (>10μm); light grey bar is nano- (2-10μm); black Bar is pico-phytoplankton (0.2-2μm).

Figure 6. Size Fractionated Photosynthesis-Irradiance parameters from Deep Chlorohyll maximum samples on AMT22 (A.) PmB, (B.) alphaB, (C.) Ek and AMT23 (D.) PmB, (E.)

alphaB, (F.) Ek. Dark grey bar is micro- (>10μm); light grey bar is nano- (2-10μm); black Bar is pico-phytoplankton (0.2-2μm).

Figure 7. In situ (filled shapes) and satellite estimated (open shapes) of micro-phytoplankton primary production (mg C m^{-2} d^{-1}) on (A.) AMT18, (B.) AMT20, (C.) AMT21, (D.) AMT22, (E.) AMT23.

Figure 8. Satellite Time Series of micro-phytoplankton primary production in (A.) North Atlantic Drift - NADR (B.) North Atlantic Gyre Province - NATL, (C.) Canary Current Coastal upwelling - CNRY, (D.) Eastern Tropical Atlantic - ETRA, (E.) Western Tropical Atlantic – WTRA, (F.) South Atlantic Subtropical Gyre - SATL, (G.) Benguela Current Coastal - BENG, (H.) South Subtropical Convergence - SSTC. Dotted line is Total PP; solid line is Micro-PP.

Figure 9. Anomaly in micro-phytoplankton primary production in (A.) NADR (B.) NATL, (C.) CNRY, (D.) ETRA, (E.) WTRA, (F.) SATL, (G.) BENG, (H.) SSTC. Solid line is regression through the anomalies. Dotted line in (G.) and (H.) is 0 to illustrate trend in regression.

Figure 10. Linear regression between monthly micro-phytoplankton primary production and export production (g C m^{-2}) calculated from Henson et al. (2011) for the (A.) NADR (filled circles; solid line) & CNRY (open circles; dashed line) (B.) NATL (filled squares; solid line) & SATL (open squares; dashed line), (C.) ETRA (filled triangles; solid line) & WTRA (open

triangles; dashed line), (D.) BENG (filled inverted triangles; solid line) & SSTC (open inverted triangles; dashed line).

Figure 11. Variation in annual micro-phytoplankton primary production (solid shapes) and export production (open shapes) in g C m^{-2} y^{-1} calculated from Henson et al. (2011) in the (A.) NADR (B.) NATL, (C.) CNRY, (D.) ETRA, (E.) WTRA, (F.) SATL, (G.) BENG, (H.) SSTC.

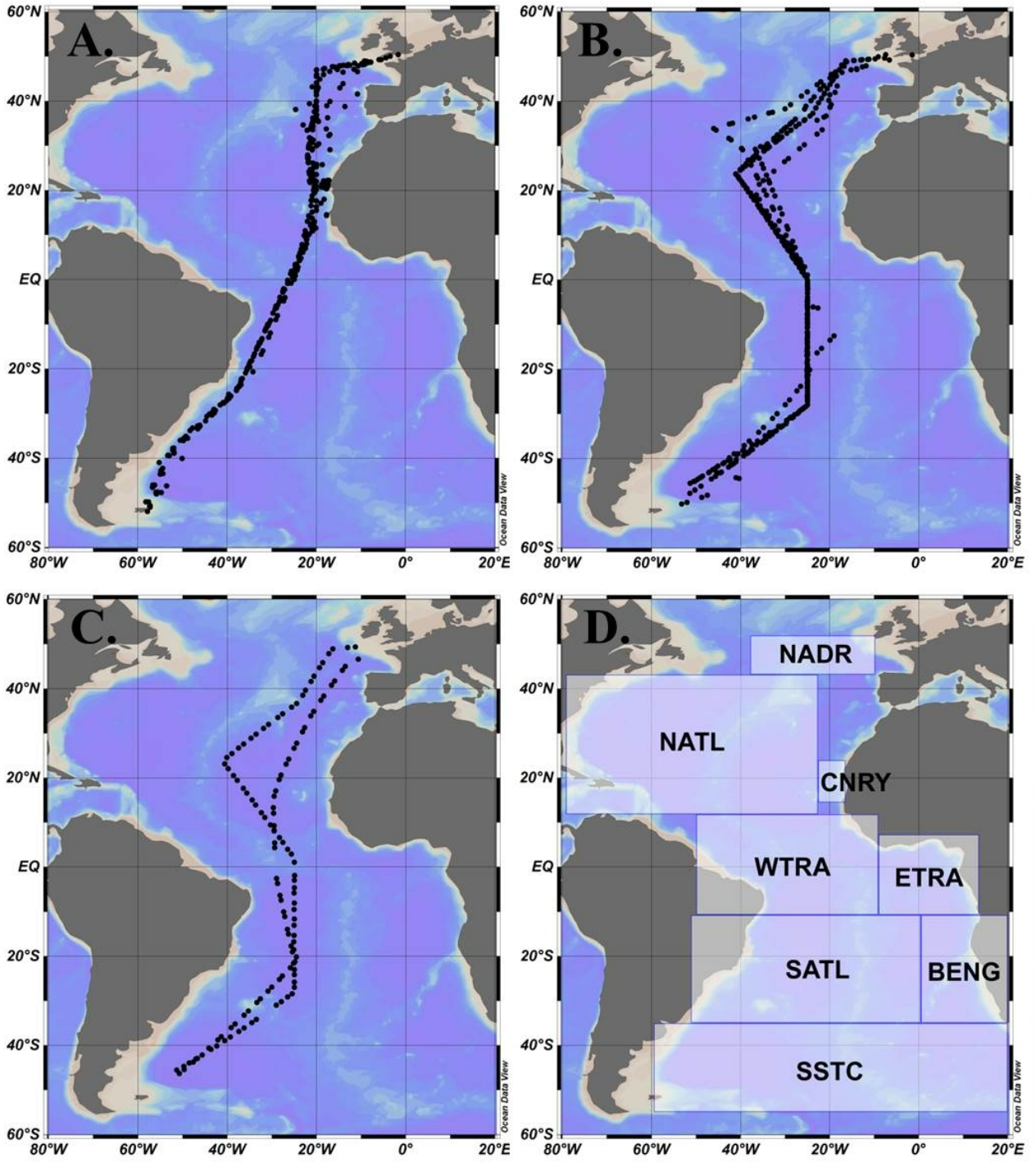
A.
B.
C.
D.
60°N
40°N
20°N
EQ
20°S
40°S
60°S
80°W
60°W
40°W
20°W
0°
20°E
Ocean Data View
NADR
NATL
CNRY
WTRA
ETRA
SATL
BENG
SSTC

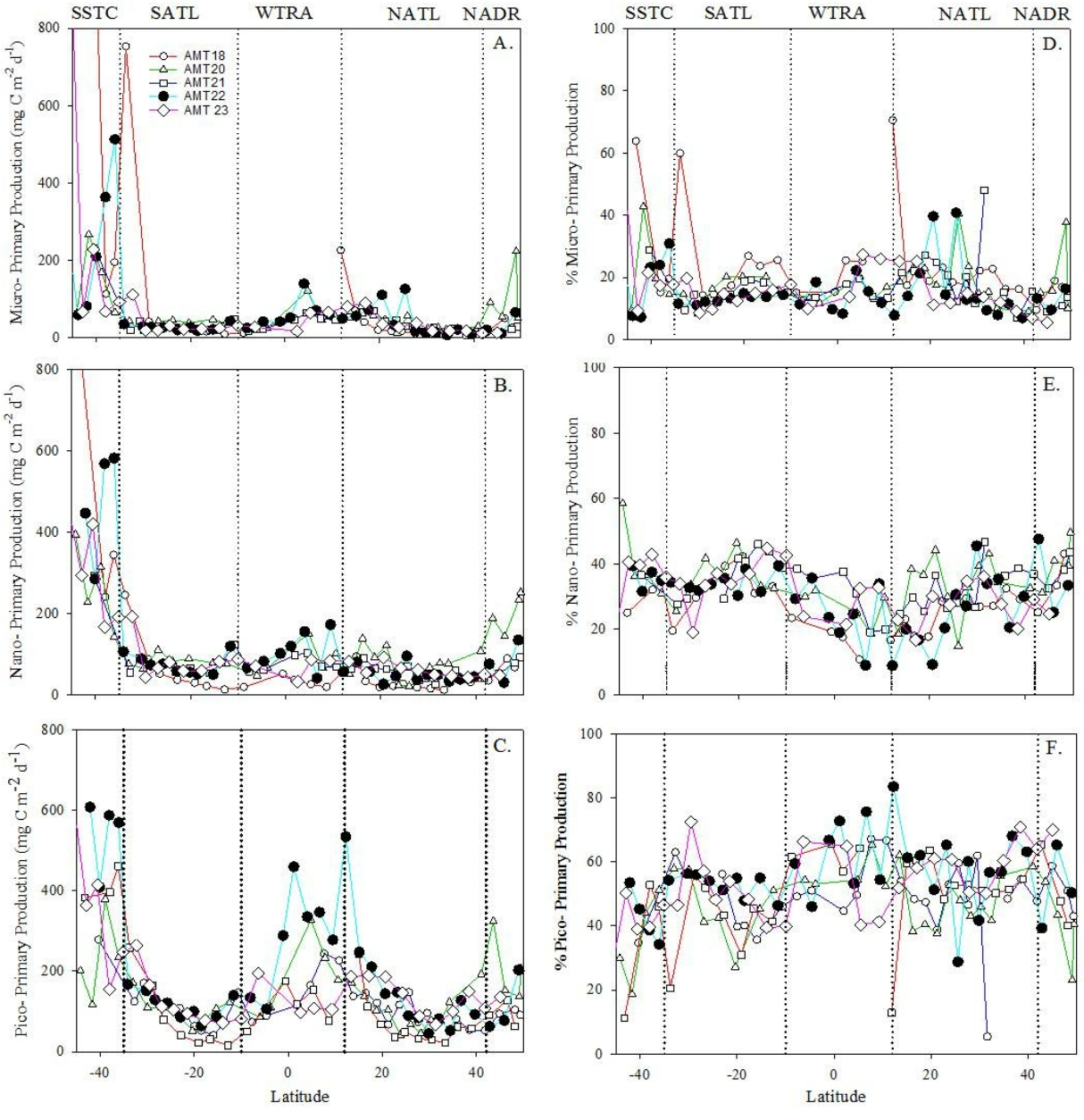
SSTC
SATL
WTRA
NATL
NADR
A.
B.
C.
D.
E.
F.
AMT18
AMT20
AMT21
AMT22
AMT 23
Micro- Primary Production (mg C m-2 d-1)
Nano- Primary Production (mg C m-2 d-1)
Pico- Primary Production (mg C m-2 d-1)
% Micro- Primary Production
% Nano- Primary Production
%Pico- Primary Production
Latitude

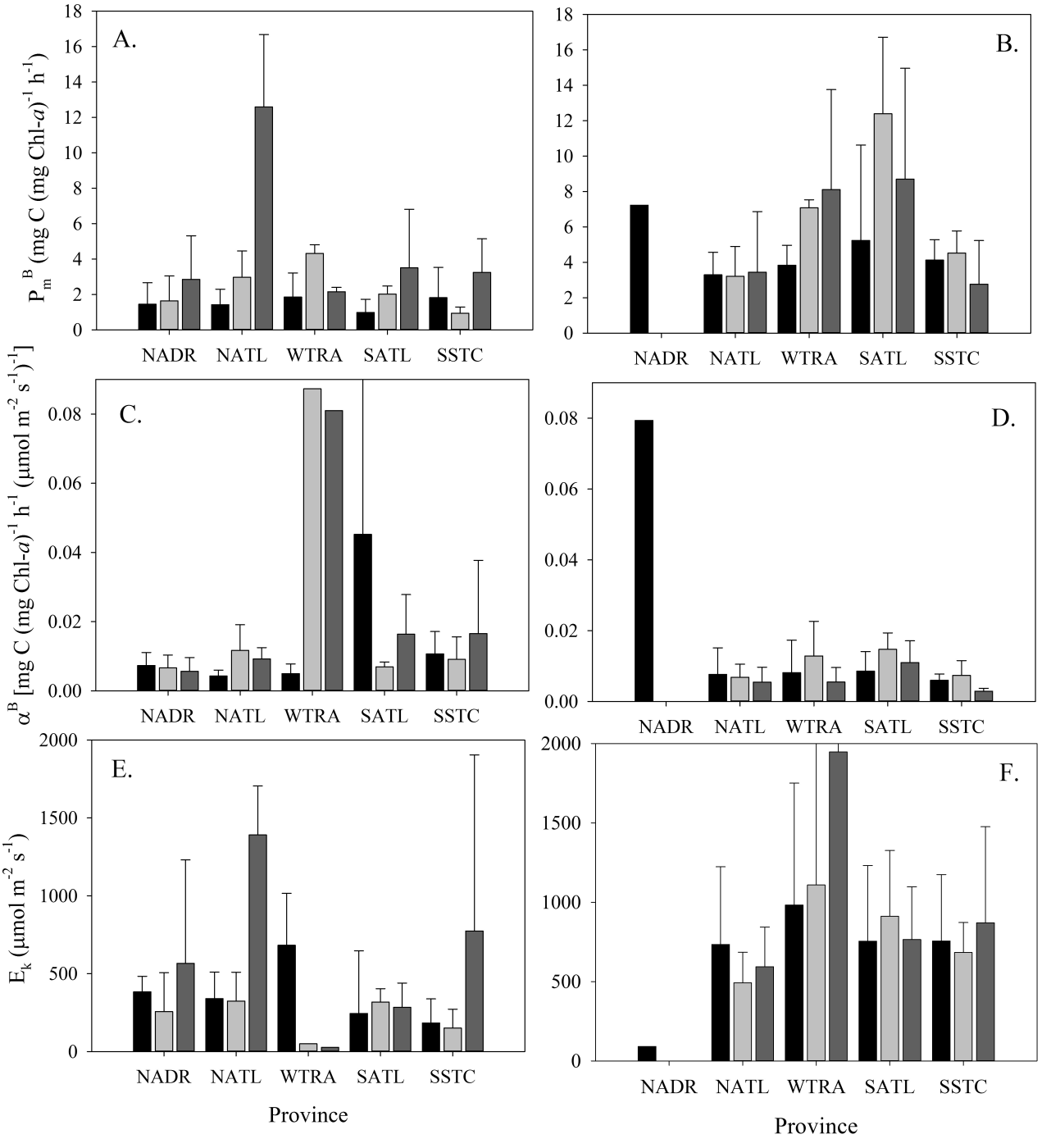
A.
B.
C.
D.
E.
F.
P_m^B (mg C (mg Chl-*a*)$^{-1}$ h^{-1})
α^B [mg C (mg Chl-*a*)$^{-1}$ h^{-1} (µmol m^{-2} s^{-1})$^{-1}$]
E_k (µmol m^{-2} s^{-1})
NADR NATL WTRA SATL SSTC
Province

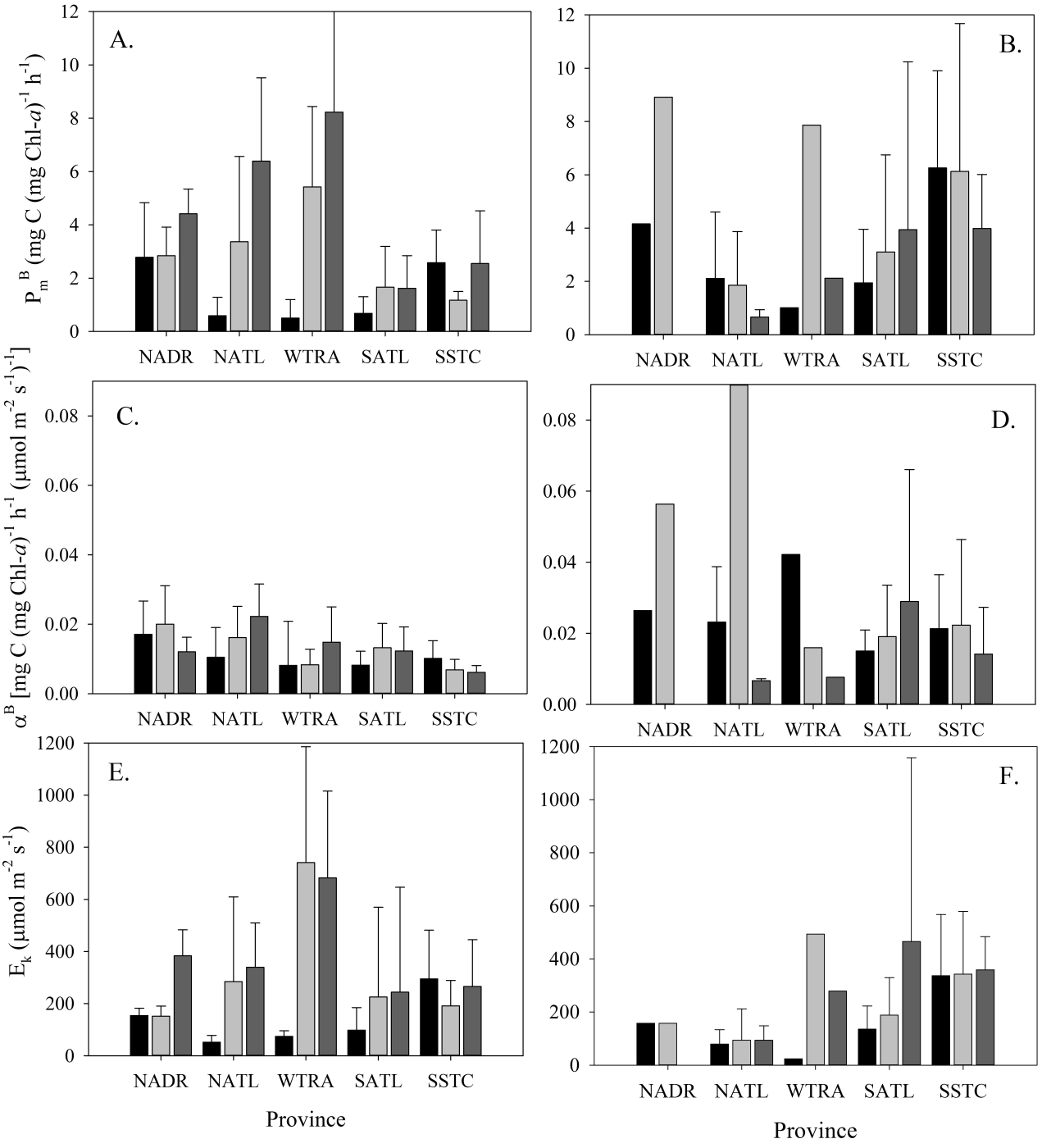
A.
B.
C.
D.
E.
F.
P_m^B (mg C (mg Chl-*a*)$^{-1}$ h^{-1})
α^B [mg C (mg Chl-*a*)$^{-1}$ h^{-1} (µmol m^{-2} s^{-1})$^{-1}$]
E_k (µmol m^{-2} s^{-1})
NADR NATL WTRA SATL SSTC
Province

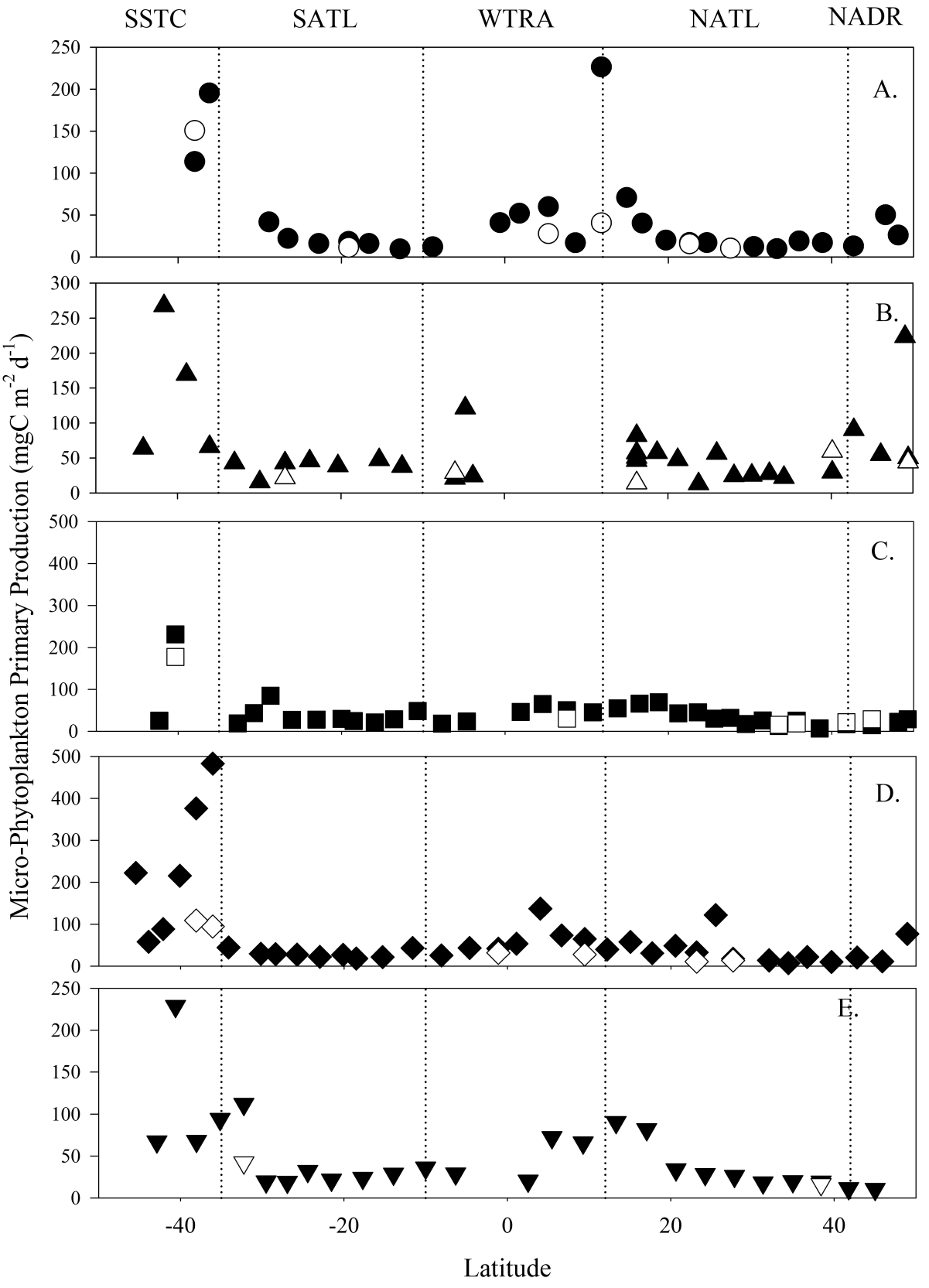
SSTC
SATL
WTRA
NATL
NADR
A.
B.
C.
D.
E.
Micro-Phytoplankton Primary Production (mgC m-2 d-1)
Latitude
-40
-20
0
20
40

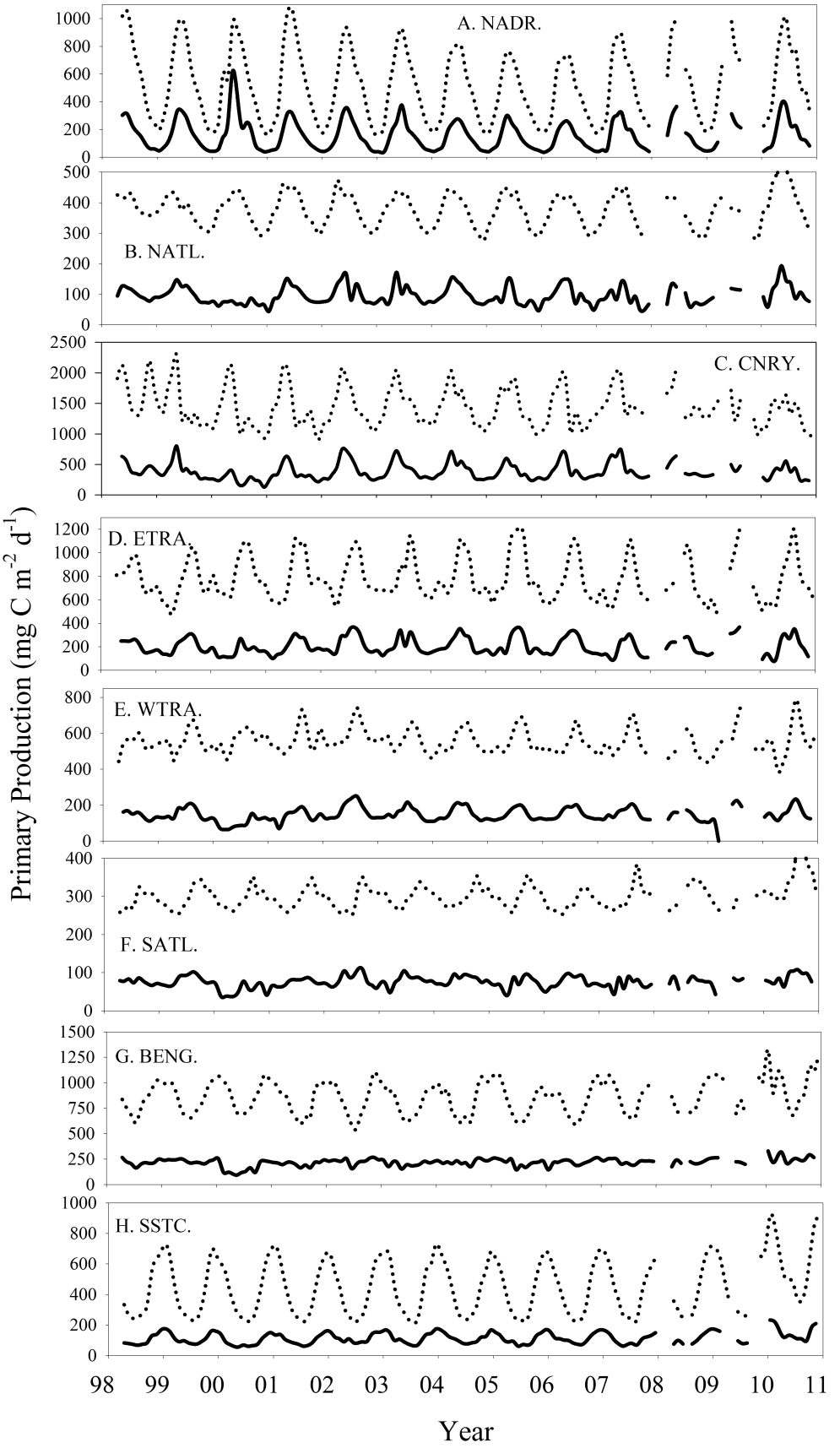
A. NADR.
B. NATL.
C. CNRY.
D. ETRA.
E. WTRA.
F. SATL.
G. BENG.
H. SSTC.
Primary Production (mg C m-2 d-1)
98
99
00
01
02
03
04
05
06
07
08
09
10
11
Year

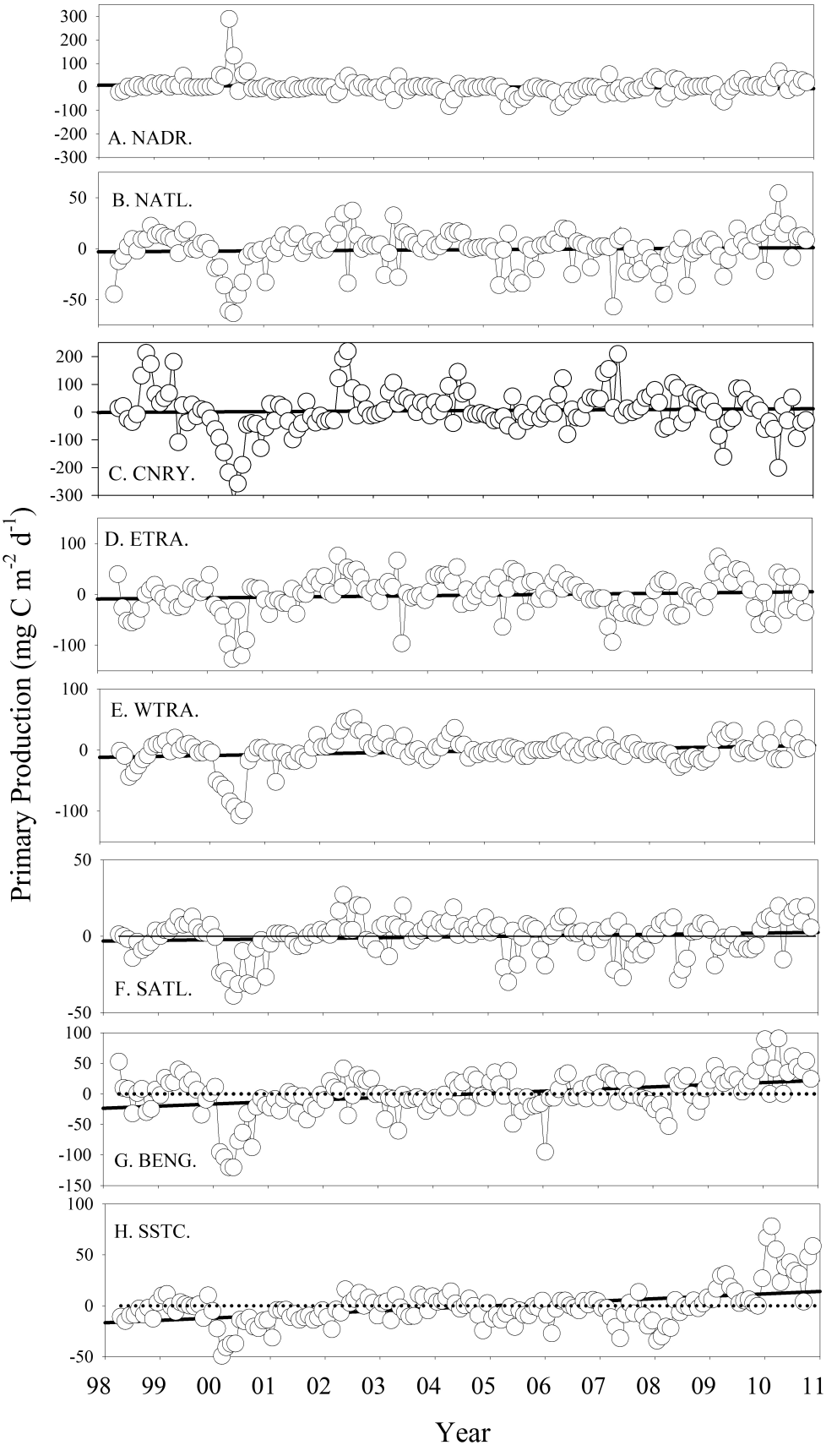
A. NADR.
B. NATL.
C. CNRY.
D. ETRA.
E. WTRA.
F. SATL.
G. BENG.
H. SSTC.
Primary Production (mg C m-2 d-1)
Year
98
99
00
01
02
03
04
05
06
07
08
09
10
11

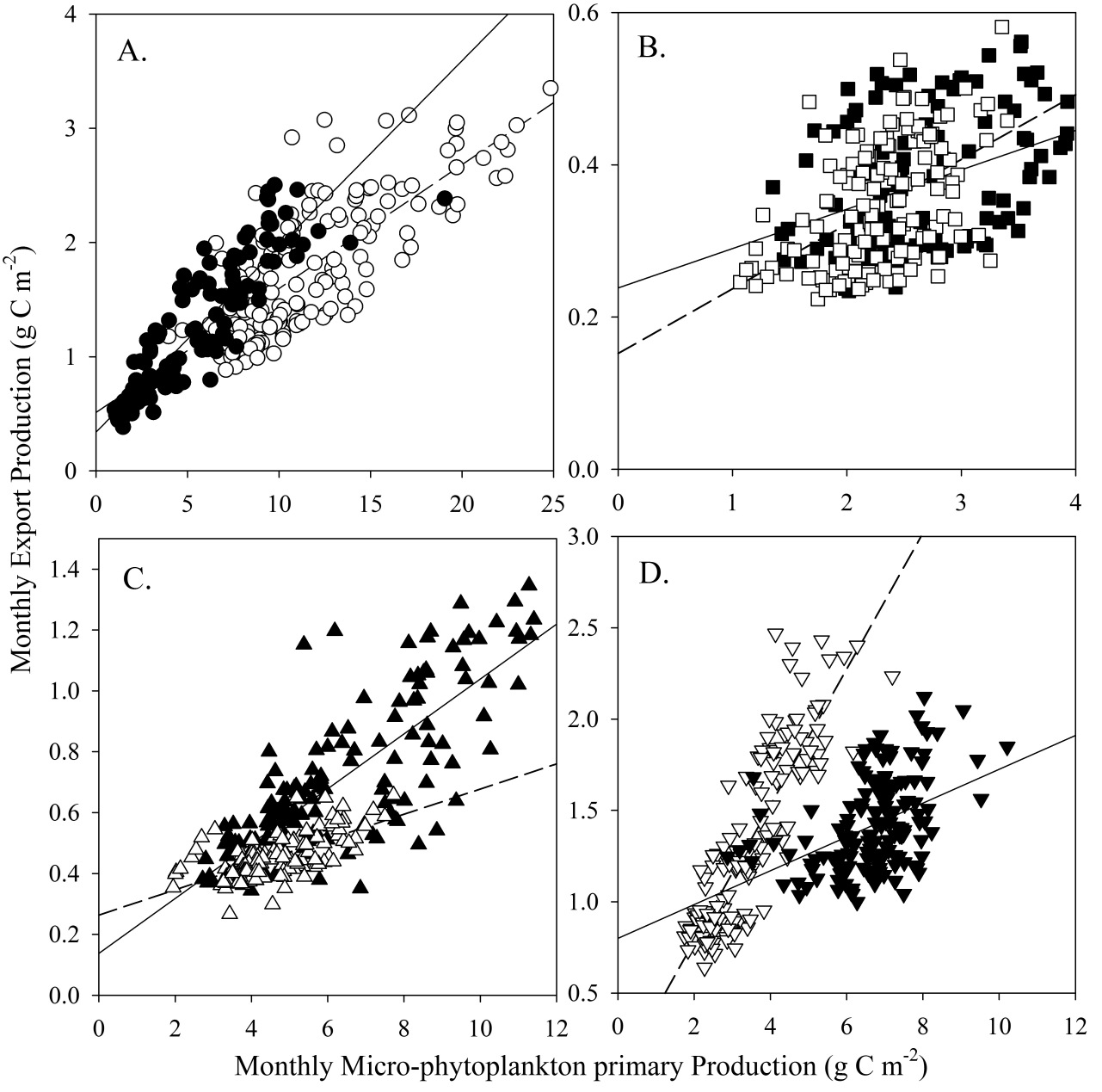
A.
B.
C.
D.
Monthly Export Production (g C m-2)
Monthly Micro-phytoplankton primary Production (g C m-2)

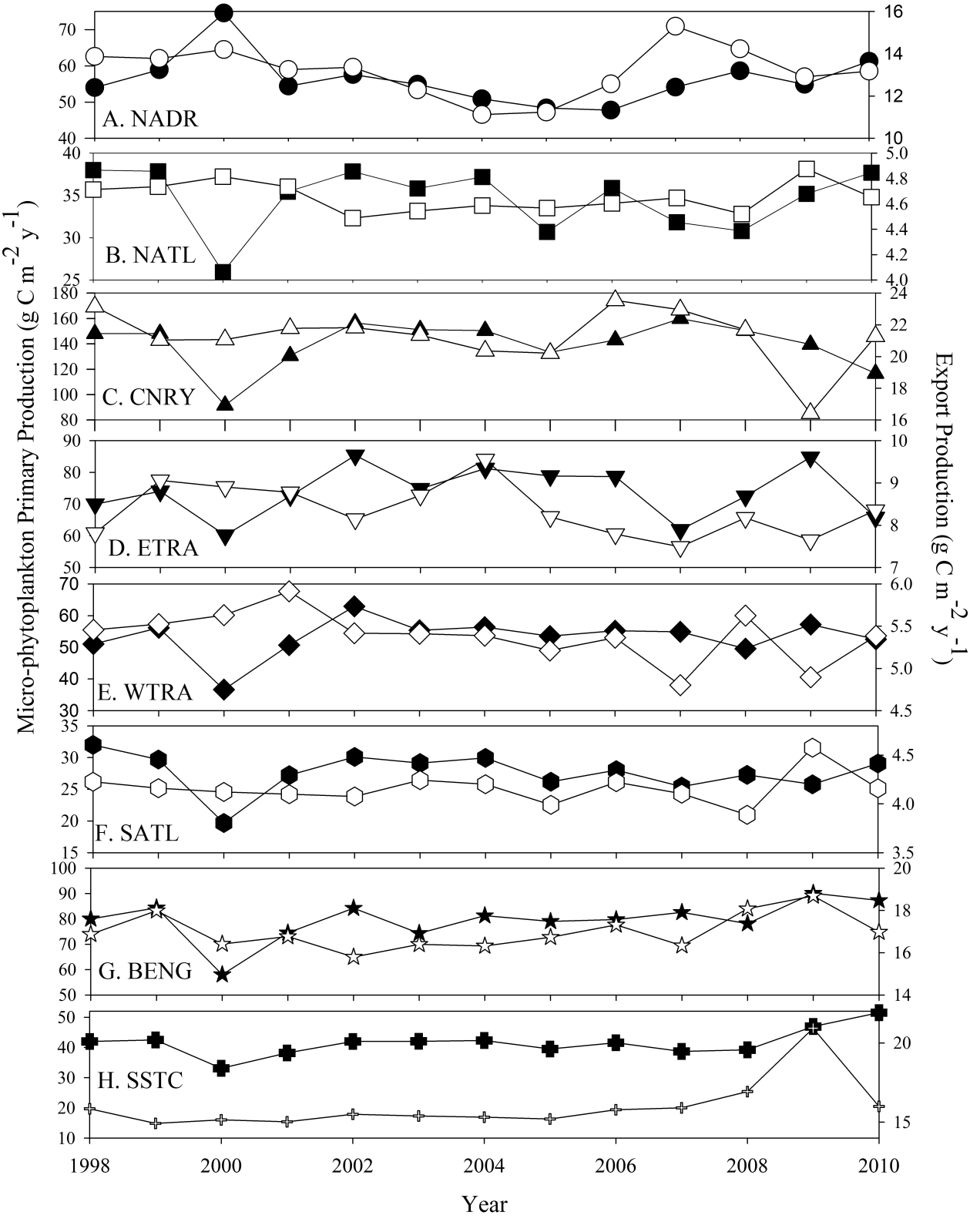
A. NADR
B. NATL
C. CNRY
D. ETRA
E. WTRA
F. SATL
G. BENG
H. SSTC
Micro-phytoplankton Primary Production (g C m-2 y-1)
Export Production (g C m-2 y-1)
Year
1998
2000
2002
2004
2006
2008
2010

Cruise	Date	Year	Filter sizes (μm)
AMT01	21 Sept – 24 Oct	1995	0.2
AMT02	22 April – 28 May	1996	0.2, 2, 20
AMT03	22 Sept – 25 Oct	1996	0.2, 2, 20
AMT04	21 April – 27 May	1997	0.2, 2, 20
AMT05	14 Sept – 17 Oct	1997	0.2, 2, 20
AMT06	14 May – 15 June	1998	0.2, 2, 20
AMT07	14 Sept – 25 Oct	1998	0.2
AMT08	25 April – 6 June	1999	0.2
AMT09	15 Sept – 13 Oct	1999	0.2
AMT10	12 April – 7 May	2000	0.2
AMT11	11 Sept – 13 Oct	2000	0.2
AMT12	12 May – 17 June	2003	0.2, 2
AMT13	10 Sept – 14 Oct	2003	0.2, 2
AMT14	26 April – 2 June	2004	0.2, 2
AMT15	19 Sept – 29 Oct	2004	0.2, 2
AMT16	19 May – 29 June	2005	0.2, 2
AMT18	3 Oct – 10 Nov	2008	0.2, 2, 10
AMT20	12 Oct – 25 Nov	2010	0.2, 2, 10
AMT21	29 Oct – 11 Nov	2011	0.2, 2, 10
AMT22	10 Oct – 24 Nov	2012	0.2, 2, 10
AMT23	7 Oct – 8 Nov	2013	0.2, 2, 10

Table 1. Dates and filter sizes for determination of size fractionated primary production on Atlantic Meridional Transect (AMT) Cruises 1 to 23.

PP **(mgC m^{-2} d^{-1})**	**AMT1-11**			**AMT12-22**		
NADR	Micro	Nano	Pico	Micro	Nano	Pico
Mean	225	218	182	52	113	133
± SD (n)	192 (21)	181 (21)	79 (21)	57 (13)	73 (13)	74 (13)
% total PP	43	42	15	17	38	44
NATL	Micro	Nano	Pico	Micro	Nano	Pico
Mean	265	132	242	37	54	111
± SD (n)	342 (42)	171 (42)	224 (42)	27 (48)	29 (48)	85 (48)
% total PP	44	22	34	18	27	55
WTRA	Micro	Nano	Pico	Micro	Nano	Pico
Mean	69	80	278	57	84	212
± SD (n)	38 (42)	41 (42)	124 (42)	33 (16)	47 (16)	115 (16)
% total PP	16	19	65	16	24	60
SATL	Micro	Nano	Pico	Micro	Nano	Pico
Mean	331	146	156	81	118	152
± SD (n)	363 (29)	153 (29)	32 (29)	147 (39)	130 (39)	141 (39)
% total PP	58	25	17	23	34	43
SSTC	Micro	Nano	Pico	Micro	Nano	Pico
Mean	ND	ND	ND	409	353	309
± SD (n)				720 (8)	237 (8)	185 (8)
% total PP				38	33	28

Table 2. Mean and standard deviation (SD) for depth integrated primary production (*PP*) and percentage of total for pico-, nano- and micro-phytoplankton during AMT1-11 and AMT12-22. N is the number of data points used to calculate the mean and SD. ND is no data.

Parameter	Surface			DCM		
NADR	Micro	Nano	Pico	Micro	Nano	Pico
Chl *a*	0.03 ± 0.01	0.076 ± 0.02	0.14 ± 0.037	0.03 ± 0.01	0.12 ± 0.024	0.35 ± 0.19
P_m^B	2.81 ± 2.01	1.95 ± 1.31	2.75 ± 2.41	2.83 ± 2.28	3.21 ± 3.03	2.33 ± 1.87
α^B	0.005 ±0.004	0.006 ±0.003	0.018 ±0.03	0.024 ±0.018	0.024 ±0.018	0.019 ±0.008
E_k	640 ± 563	389 ± 335	368 ± 465	255 ± 189	125 ± 51	117 ± 61
NATL	Micro	Nano	Pico	Micro	Nano	Pico
Chl *a*	0.02 ± 0.02	0.024 ± 0.01	0.074 ± 0.05	0.02 ± 0.012	0.048 ± 0.02	0.23 ± 0.11
P_m^B	8.82 ± 5.78	4.23 ± 2.29	2.68 ± 1.52	5.94 ± 5.17	3.99 ± 3.51	1.08 ± 1.63
α^B	0.007 ±0.004	0.01 ±0.007	0.007 ±0.006	0.02±0.01	0.047 ±0.019	0.016 ±0.015
E_k	1328 ± 1026	588 ± 648	587 ± 480	460 ± 478	261 ± 281	61 ± 40
WTRA	Micro	Nano	Pico	Micro	Nano	Pico
Chl *a*	0.01 ± 0.01	0.026 ± 0.03	0.082 ± 0.05	0.026 ± 0.01	0.07 ± 0.045	0.28 ± 0.13
P_m^B	5.15 ± 4.08	10.07 ± 5.3	3.82 ± 4.51	5.63 ± 5.12	3.71 ± 2.96	1.75 ± 2.11
α^B	0.02 ±0.03	0.024 ±0.03	0.006 ±0.004	0.022 ± 0.03	0.011 ±0.009	0.011 ±0.010
E_k	648 ± 486	780 ± 468	629 ± 462	494 ± 380	483 ± 443	146 ± 161
SATL	Micro	Nano	Pico	Micro	Nano	Pico
Chl *a*	0.02 ± 0.04	0.06 ± 0.094	0.09 ± 0.133	0.034 ± 0.04	0.10 ± 0.15	0.20 ± 0.12
P_m^B	3.20 ± 3.18	2.55 ± 1.31	1.21 ± 1.02	2.18 ± 1.66	2.88 ± 3.49	1.97 ± 3.10
α^B	0.01 ±0.01	0.007 ±0.002	0.041 ±0.011	0.013 ± 0.01	0.016 ±0.013	0.012 ±0.010
E_k	306 ± 154	374 ± 161	279 ± 210	270 ± 356	260 ± 311	120 ± 102
SSTC	Micro	Nano	Pico	Micro	Nano	Pico
Chl *a*	0.03 ± 0.05	0.084 ± 0.11	0.13 ± 0.16	0.046 ± 0.05	0.13 ± 0.17	0.24 ± 0.12
P_m^B	5.41 ± 4.89	3.69 ± 1.44	2.13 ± 1.74	3.38 ± 2.08	5.17 ± 4.21	3.21 ± 3.69
α^B	0.009 ±0.01	0.007 ±0.003	0.06 ±0.14	0.012±0.01 7	0.015 ±0.019	0.015 ±0.015
E_k	751 ± 475	546 ± 238	535 ± 553	423 ± 420	500 ± 328	204 ± 194

Table 3. Mean and standard deviation for Chl a (mg m^{-3}) and the photo-physiological parameters; the maximum photosynthetic rate (P_m^B) (mg C (mg Chl-*a*)$^{-1}$ h^{-1}), the light-limited photosynthetic rate (α^B)

(mg C (mg Chl-*a*) $^{-1}$ h $^{-1}$ (µmol photons m $^{-2}$ s $^{-1}$) $^{-1}$) and the light saturation parameter (E_k) (µmol photons m $^{-2}$ s $^{-1}$) for pico-, nano- and micro-phytoplankton.

Reference	Region	Pore size (µm)	P_m^B	α^B	E_k
Tilstone et al. (this study) n=124	Atlantic Ocean	*Micro* >10 *Nano* 2 - 10 *Pico* 0.2 - 2	4.54 (0.08 – 17.13) 4.15 (0.05 – 18.47) 2.29 (0.07 – 17.92)	0.013 (0.002 – 0.085) 0.014 (0.002 – 0.087) 0.018 (0.001 – 0.079)	578 (6 – 3554) 448 (5 – 2173) 332 (2 – 1795)
Uitz et al. (2008) n=902	NATL, CNRY, equatorial Pacific, Med Sea	***Micro* >10 ***Nano* 2 - 10 **Pico* 0.2 - 2	4.26 2.94 3.75	0.032 0.026 0.007	ND
Claustre et al. (2005) n = 334	Atlantic Ocean - NATL	*† Micro* >20 *Nano* 2 - 10 *Pico* 0.2 - 2	6.27 2.38 0.13	0.093 0.046 0.014	ND
Platt et al. (1983) n=11	Atlantic Ocean - NATL	*Nano+Micro* >1 *Pico* 0.2 - 1	0.49 (0.24 – 0.92) 0.68 (0.25 - 1)	0.038 (0.014 – 0.068) 0.074 (0.025 – 0.1)	∇14 (7 – 19) 9.5 (6 – 14)
Tilstone et al. (1999) n=54	NW Iberian Upwelling	*Micro* >20 *Pico+ Nano* 0.2 - 20	2.26 (0.61 – 7.41) 3.09 (0.86 – 6.27)	0.015 (0.005 – 0.029) 0.024 (0.008 – 0.037)	ND
Figueiras et al. (2014) n=94	NW Iberian Upwelling	***Micro* >10 **Nano* 2 - 10 **Pico* 0.2 - 2	3.58 1.55 4.25	0.015 0.021 0.036	ND
Moran & Sharek (2015) n=11	Bay of Biscay	*Nano+Micro* >2 *Pico* 0.2 - 2	3.62 (1.98-5.60) 5.41 (0.88-7.17)	0.024 (0.003 - 0.026) 0.031 (0.002 – 0.052)	179 (98 – 291) 282 (104 – 572)
Li et al. (2011) n=104	North Pacific Subtropical Gyre	*Nano+Micro* >2 *Pico* 0.2 - 2	5.57 (1.3 - 14.2) 2.45 (0.9 – 4.5)	0.04 (0.01 – 0.1) 0.03 (0.01 – 0.1)	130 (25 - 319) 110 (27 - 286)
Toon et al. (2000) n=19	Northern Arabian Sea	*Micro* >20 *Nano* 2 - 20 *Pico* 0.2 - 2	3.5 (1.05 - 5.86) 4.0 (1.79 - 5.75) 4.28 (ND)	0.017 (0.008 – 0.013) 0.017 (0.01 – 0.023) 0.038 (ND)	ND
Segura et al. (2013) n=70	Argentine Sea	*Micro* >5 *Nano+ Pico* <5	3.17 (ND) 2.40 (ND)	0.15 (ND) 0.19 (ND)	ND
deMadariaga and Joint (1994) n=11	Celtic Sea	*Micro* >5 *Nano* 1 - 5 *Pico* 0.2 - 1	3.44 (1.75 – 8.26) 4.10 (1.80 – 9.58) 8.49 (3.84 – 17.22)	0.013 (0.007 – 0.033) 0.024 (0.009 – 0.043) 0.219 (0.044 – 0.68)	257 (195 – 390) 184 (103 – 300) 105 (19 - 236)
Barnes et al. (2014)	Western English	*Micro* >10	4.15 (1.06 - 17.38)	0.015 (0.002-0.049)	332 (84-2186)

n=87	Channel	*Nano* 2 - 10 *Pico* 0.2 - 2	4.10 (0.44 – 26.10) 8.09 (1.66 – 24.55)	0.019 (0.001 – 0.092) 0.044 (0.004 – 0.223)	259 (44 – 1569) 278 (13 – 1163)

Table 4. Comparison of range and Mean in the size-fractionated photosynthetic parameters; P_m^B (mg C (mg Chl-*a*)$^{-1}$ h^{-1}), α^B (mg C (mg Chl-*a*) $^{-1}$ h $^{-1}$ (µmol photons m $^{-2}$ s $^{-1}$) $^{-1}$) and the E_k (µmol photons m $^{-2}$ s $^{-1}$) for pico-, nano- and micro-phytoplankton, from our data with other studies. N is the total number of *PE* curves per size fraction. ***micro- is derived from the weighted phytoplankton pigment concentrations of fucoxanthin + peridinin, **nano- from alloxanthin + 19-hex + 19-but, *pico- from zeaxanthin + Chl *b* + divinyl- Chl *b*. † size fraction values derived from correlations between % phytoplankton biomass and *PE* parameters. ∇ E_k values are in W m^{-2}.

Province	Model II Linear regression (g C m^{-2})	r^2
NADR	export P = micro-PP * 0.16 + 0.34	0.83
CNRY	export P = micro-PP * 0.11 + 0.51	0.58
NATL	export P = micro-PP * 0.05 + 0.24	0.27
SATL	export P = micro-PP * 0.08 + 0.15	0.24
ETRA	export P = micro-PP * 0.09 + 0.14	0.64
WTRA	export P = micro-PP * 0.04 + 0.26	0.45
BENG	export P = micro-PP * 0.09 + 0.80	0.19
SSTC	export P = micro-PP * 0.37 + 0.04	0.76

Table 5. Linear regression between monthly micro-phytoplankton Primary Production and Export Production (g C m^{-2}) estimated from SeaWiFS Ocean Colour data. Export production was estimated from the Thorium-234 export production using the algorithm of Henson et al. (2011).

Research highlights:

- Spatial and temporal changes in micro-phytoplankton production (micro-PP) were assessed.
- Micro-PP was highest in the South Subtropical Convergence (SSTC) constituting 25 % of the total PP.
- Micro-phytoplankton had the highest maximum photosynthetic rates.
- Size-fractionated photosynthetic parameters were used to calibrate a micro-PP satellite model.
- The model applied to SeaWiFS data showed an increase in micro-PP in the Benguela Upwelling and SSTC.
- In the SSTC, 39 % of micro-PP was estimated to be exported out of the photic zone.